Enhanced Nonlinear Truss Model for Capturing Combined Earthquake and Fire Effects in RC Structures

Amy Melissa Allen

Thesis submitted to the faculty of the Virginia Polytechnic Institute and State University in partial fulfillment of the requirements for the degree of

Master of Science

In

Civil and Environmental Engineering

Ioannis Koutromanos, Chair

Carin L. Roberts-Wollmann

Roberto T. Leon

May 6, 2015

Blacksburg, VA

Keywords: Truss Model, Earthquake, Fire, Reinforced Concrete

Enhanced Nonlinear Truss Model for Capturing Combined Earthquake and Fire Effects in RC Structures

Amy Melissa Allen

ABSTRACT

Post-earthquake fires can negatively affect the safety and collapse probability of Reinforced Concrete (RC) structures. At present, there has been no systematic effort to assess the performance of RC structures for combined earthquake and fire effects. Developing appropriate guidelines for this scenario requires simulation tools that can accurately capture material behavior during cyclic loading and at elevated temperatures. Ideally, simulation tools must also be conceptually simple and computationally efficient to allow extensive parametric analyses.

The goal of the present study is to enhance a previously established modeling approach so that it can describe the performance of RC structures for both cyclic loading and changes in material behavior due to elevated temperatures. The modeling approach is based on the nonlinear truss analogy and has been extensively validated for cyclic loading of RC shear walls and columns. The constitutive models for concrete and reinforcing steel are enhanced with the capability to account for the effect of elevated temperatures. The enhanced material models are validated using experimental data for concrete and steel at elevated temperatures. The capability of the proposed model to analyze structural-level behavior is verified and compared with experimental testing. The method is also endowed with the capability to describe the time-dependent heat conduction in a fire simulation. The use of the enhanced nonlinear truss model is more advantageous than refined finite element models because of its computational efficiency and conceptual simplicity.

Acknowledgements

I would like to thank my adviser, Dr. Ioannis Koutromanos, for his advice and feedback throughout this process. He taught me to set high standards and to think critically about my research. I would also like to thank my other committee members, Dr. Carin Roberts-Wollmann and Dr. Roberto Leon, for their time and helpful feedback.

Gratitude also goes to my family for their unending love and support. I would not be where I am today without them. I would like to thank my friends that provided much needed encouragement and laughter this year. I would also like to give praise to God, whose grace and steadfast love endure forever (Psalm 106).

Table of Contents

List of Figures

List of Tables

Notation

ACI	American Concrete Institute
AISC	American Institute of Steel Construction
AS	Australian Standard
ASCE	American Society of Civil Engineers
ASTM	American Society for Testing and Materials
CEN	European Committee for Standardization
EC	Eurocode
FDS	Fire Dynamics Simulator
FEA	Finite Element Analysis
FEAP	Finite Element Analysis Program
FEMA	Federal Emergency Management Agency
FSI	Flexure-Shear Interaction
HSC	High Strength Concrete
IO	Immediate Occupancy
NEHRP	National Earthquake Hazards Reduction Program
NIST	National Institute of Standards and Technology
NSC	Normal Strength Concrete
PEF	Post-Earthquake Fire
RC	Reinforced Concrete
TMS	The Masonry Society
$B^{(e)}$	Gradient temperature matrix for element e
c_p	Specific heat

E_0	Young's modulus at room temperature
E_T	Young's Modulus at temperature T
F(T)	Stress reduction factor for concrete
f_{cm}	Compressive strength of concrete at elevated temperature
f_{cmo}	Compressive strength of concrete at room temperature
$F_E(T)$	Reduction factor for modulus of elasticity of reinforcing steel under elevated temperatures
f_{sT}	Stress in steel at temperature T
f_{su}	Ultimate stress in reinforcing steel
f_{t0}	Tensile strength of concrete at room temperature
f_{tT}	Tensile strength of concrete at elevated temperature T
f_y	Yield strength of reinforcing steel
$F_y(T)$	Stress reduction factor for reinforcing steel under elevated temperature
f_{y0}	Yield strength of steel at room temperature
f_{yT}	Yield strength of steel at elevated temperature T
J	Jacobian for iterative solution of nonlinear scalar equation
k_t	Tensile stress reduction factor for concrete
k_{tr}	Transient strain constant
$[N^{(e)}]$	Shape function array for element e
{q}	Heat flux vector
r	Residual for iterative solution of nonlinear scalar equation
s	Heat source term for heat conduction problem
t	Time
T	Temperature

$\{T_0\}$	Initial nodal temperature vector
β	Reduction factor for transverse tensile strain
Γ_q	Natural boundary on which flux is prescribed
Γ_T	Essential boundary on which temperature is prescribed
ε_{cr}	Creep strain
ε_m	Mechanical strain
ε_{sh}	Strain at which strain hardening begins in reinforcing steel
$\varepsilon_{s,th}$	Thermal strain in reinforcing steel
ε_{su}	Ultimate strain of reinforcing steel
ε_t	Transverse tensile strain
ε_{th}	Thermal strain
ε_{total}	Total strain
ε_{tr}	Transient strain in concrete under elevated temperatures
ε_{uT}	Ultimate strain in steel at temperature T
ε_y	Yield strain in reinforcing steel
κ_{fm0}, κ_{fm1}, κ_{fm2}, κ_{fm3}	Regression coefficients for compressive stress reduction factor
λ_c	Thermal conductivity of concrete
ρ	Density of concrete
ρ_0	Density of concrete at room temperature
σ	Stress
σ_0	Stress at room temperature obtained from concrete constitutive law
σ_c	Compressive stress in concrete
σ_{EC}	Stress from Eurocode steel constitutive law

σ_{ex}	Stress from constitutive law implemented in present study for reinforcing steel
σ_t	Tensile stress in concrete
σ_T	Stress in concrete at temperature T
σ_{u0}	Compressive strength of concrete at room temperature
σ_{uT}	Compressive strength of concrete at temperature T
τ	Shear stress in concrete

1 Introduction

Earthquake and fire are two extreme events that can occur during a structure's service life. The damage due to earthquakes and fires can have significant effects on the structure's load-carrying capacity and serviceability. A particularly extreme scenario is the occurrence of fire after a strong earthquake. This can occur when gas or electrical lines are damaged during an earthquake. Current design procedures involve designing and detailing structural systems for the effects of earthquakes and fires separately, but not in combination. Additionally, the design procedures for fire effects are often based on prescriptive requirements rather than performance-based design, particularly in the United States. These methods of design may not be adequate if a structure is subjected to the combined effects of a post-earthquake fire. The 1906 San Francisco earthquake, the 1923 Tokyo earthquake, and the 1995 Kobe, Japan earthquake are all examples when post-earthquake fires caused significant structural damage (Mousavi et al. 2008).

A method is needed to predict the performance of reinforced concrete structures to the combined effects of earthquake and fire, but there has been limited experimental or analytical research in this subject area. The present study aims to provide a simulation method for RC buildings subjected to seismic loading and post-earthquake fire. The method is an enhancement of an analysis approach based on the nonlinear truss analogy. The advantage of the truss analogy for reinforced concrete is that uniaxial constitutive laws can be used, which are more readily available from test data for cyclic loading and elevated-temperature testing. Furthermore, truss models are more computationally efficient and better at capturing shear failure than traditional finite element models. In this study, an existing nonlinear truss model that was developed for earthquake analysis is modified to incorporate the effects of elevated temperature (i.e. fire) on

the concrete and steel material behavior. The proposed model is then validated using existing experimental data.

2 Literature Review

2.1 Effect of Elevated Temperatures on Concrete

Kodur et al. (2008) classified the concrete material properties into three categories: thermal, mechanical, and material-specific behavior (such as spalling in concrete). The thermal properties, such as thermal conductivity and specific heat, affect the temporal and spatial distribution of temperature in a concrete member subjected to a fire. The mechanical properties describe the changes in material strength and deformability due to elevated temperatures. Spalling in concrete, which can affect member capacity and rate of temperature rise in the reinforcing steel, is affected by such factors as relative humidity, rate of fire temperature rise, and strength of concrete. Kodur et al. (2008) compared several models for concrete properties at elevated temperatures, including those in Eurocode 2 (CEN 2004), ASCE 78 Manual (ASCE 1992), and several experimental studies. Eurocode 2 does not take into account the effect of aggregate type on the thermal properties of concrete, whereas ASCE 78 establishes separate models for thermal properties of concretes made with siliceous aggregate (e.g., sandstone, quartz) and carbonate aggregate (e.g., limestone, dolomite). Conversely, Eurocode 2 provides models for the strength reduction in both normal strength concrete (NSC) and high strength concrete (HSC), whereas ASCE focuses on NSC only.

Under elevated temperatures (such as fire scenarios), concrete undergoes degradation in strength and increase in deformability (Knaack et al. 2011; Kodur et al. 2008; Youssef and Moftah 2007). Extensive research has been performed to determine the influence of temperature on the compressive strength of concrete (Anderberg and Thelandersson 1976; Knaack et al. 2009; Zaidi et al. 2012). The change in compressive strength is affected by several factors, such as aggregate type, whether or not the concrete is stressed during heating, and whether the

concrete is normal strength or high strength. Example relationships for compressive strength as a function of temperature from Knaack et al. (2009) are presented in Figure 2.1.

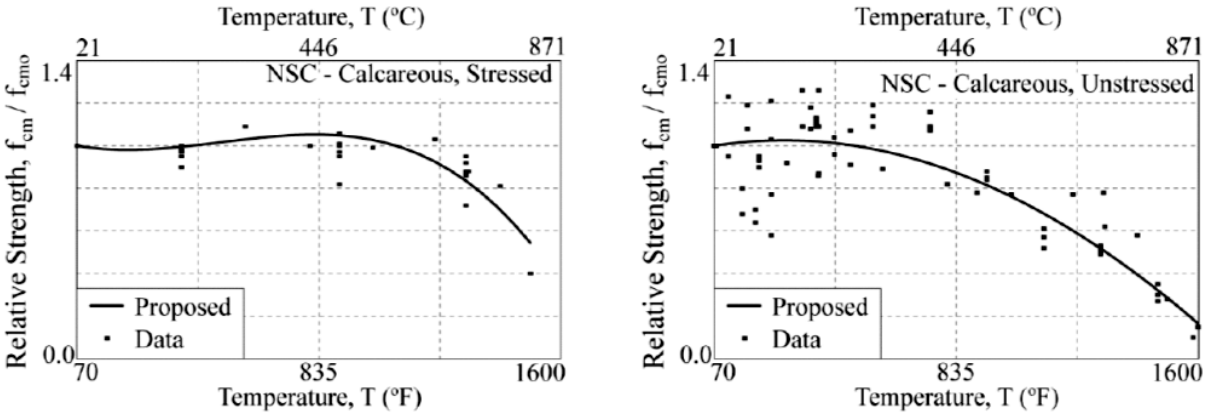

(a) (b)

Figure 2.1. Compressive strength as a function of temperature for normal strength calcareous concrete that is (a) stressed during heating and (b) unstressed during heating, proposed by Knaack et al. (2009).

Knaack, A. M., Kurama, Y. C., and Kirkner, D. J. (2009). *Stress-Strain Properties of Concrete at Elevated Temperatures, Report #NDSE-09-01*. *Structural Engineering Research Report*. Used under fair use, 2015.

At elevated temperatures, concrete also experiences temperature-dependent strains due to changes in the chemistry and microstructure of the material. The strain under elevated temperatures can be considered as the summation of stress-induced mechanical strain (ε_m), creep strain (ε_{cr}), thermal strain (ε_{th}), and transient strain (ε_{tr}), as illustrated in Figure 2.2. For concrete under a compressive load, thermal strain will be tensile, i.e. positive, and the other three strain components will be compressive, i.e. negative. Creep is an increase in strain due to viscoelastic effects, and it becomes exacerbated by elevated temperatures (Knaack et al. 2009). Thermal strain is a result of the autogenous thermal expansion of concrete, and it is only dependent on temperature. Transient strain is a stress- and temperature-dependent strain that develops during the first heating cycle of concrete. It only develops if the concrete is stressed during heating, and

it applies for compressive loading only. Sadaoui and Khennane (2009) suggested that transient strain is the result of thermo-mechanical interactions in the cement paste. Anderberg and Thelandersson (1976) noted that transient strain is irrecoverable (i.e. transient strain does not return to zero upon cooling) and proposed that the transient strain was a result of chemical reactions within the concrete. Bažant and Kaplan (1996) included transient strain under the category of creep strain. They attributed this combined creep strain to the breaking and reforming of bonds in the cement gel at elevated temperatures and to the acceleration of dehydration in the cement that occurs during heating (Bažant and Kaplan 1996). Li and Purkiss (2005) summarize several expressions for the different strain components from literature and suggest that creep strain can generally be neglected during the relatively short time period of typical fires. Transient strain can be a significant portion of the total strain during fire, so it must be included in analysis (Anderberg and Thelandersson 1976). The temperature-dependent strains can be included in material models either implicitly, i.e. by modifying the stress-strain curve for elevated temperatures, or explicitly by modeling temperature-dependent strains individually and adding them to the mechanical strain.

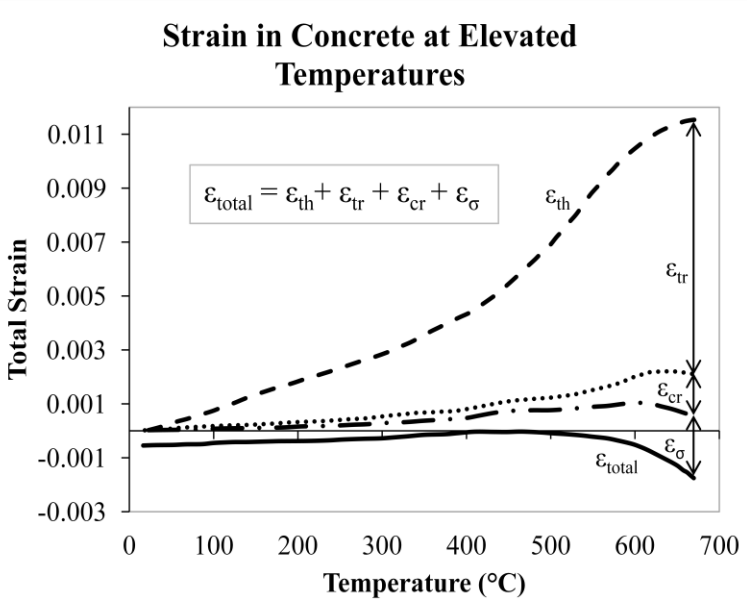

Figure 2.2. Variation of strain components with temperature, adapted from Anderberg and Thelandersson (1976).

Youssef and Moftah (2007) present an overview of available models for concrete at elevated temperatures. These models include expressions for the impact of temperature on compressive strength, the strain at peak stress, initial modulus of elasticity, thermal strain, transient strain, tensile strength, and bond strength of reinforcing bar. After comparing these models with existing experimental data, Youssef and Moftah (2007) chose the most accurate model for each property and incorporated these properties into existing stress-strain constitutive laws for concrete at ambient temperatures. The two models proposed by Youssef and Moftah (2007) for the compressive constitutive relationship at elevated temperatures matched experimentally-obtained stress-strain curves well and took into account several factors, such as preloading, aggregate type, and confinement. Youssef and Moftah (2007) noted that compressive loading on a concrete specimen reduces the temperature effects on the compressive strength and concrete strain at peak stress, but increases the transient strains in the material.

Zaidi et al. (2012) analyzed the effects of confinement on cylinders that are exposed to elevated temperatures. For the temperature range up to 800°C, larger amounts of confining reinforcement (i.e. smaller spacing) led to increased strength and ductility. The strength of the confining reinforcement (510 MPa / 74 ksi versus 726 MPa / 105 ksi) did not have a significant effect on the concrete performance. The specimens that were composed of HSC demonstrated a faster post-peak strength degradation when compared with normal strength concrete specimens. At temperatures of 600°C, the confined specimens showed reductions in strength of 19-28%, whereas the strength reduction for the unconfined specimens exceeded 50%. The confinement helped to reduce cracking due to thermal expansion and spalling at elevated temperatures.

Bažant and Kaplan (1996) discussed two mechanisms that can cause increased spalling in concrete at elevated temperatures. The first mechanism is the increased tensile stresses due to water vapor pressure. As the temperature increases, the water in the pores of the concrete evaporates and expands. When trapped within the pores, the vapor causes tensile stresses in the concrete. If the tensile stress is greater than the tensile strength of the concrete, then spalling occurs. The second mechanism is the increase in compressive stress due to thermal expansion that occurs under localized heating. When only a portion of a concrete structure is heated, the surrounding room-temperature concrete can exert restraining forces on the heated concrete to counteract the thermal expansion. This restraint causes compressive stresses to increase in the heated concrete, and this can lead to spalling.

Ulm et al. (1999) studied the causes of the extensive thermal spalling that occurred during a fire in 1996 in the Chunnel, a rail tunnel connecting England and France. The investigation and analysis revealed that the spalling was primarily caused by the stresses that develop due to restrained thermal expansion. When the surface of the tunnel concrete was heated

during the fire, compressive restraint forces developed in the orthoradial and longitudinal directions. This biaxial stress state caused cracking planes parallel to the plane of load application, leading to spalling of the surface concrete. These results illustrate the need to account for thermal strain and the resulting stresses that can develop due to thermal restraint.

2.2 Effect of Elevated Temperature on Reinforcing Steel

Elevated temperatures can also affect the strength and deformability of reinforcing steel. Steel at ambient temperature exhibits a yield plateau, but at elevated temperatures the yield plateau disappears, and there is not a distinct yield point (Purkiss and Li 2013). This was experimentally observed in the stress-strain curves by Harmathy and Stanzak (1970), as shown in Figure 2.3 for an ASTM A36 steel sample. According to the relation presented by Purkiss and Li (2013), significant reduction in the modulus of elasticity of reinforcing steel occurs around 600 degrees C. Strains in the steel are composed of stress-induced mechanical strain, thermal strain, and creep strain. The creep strain does not become significant unless the temperature exceeds 450°C.

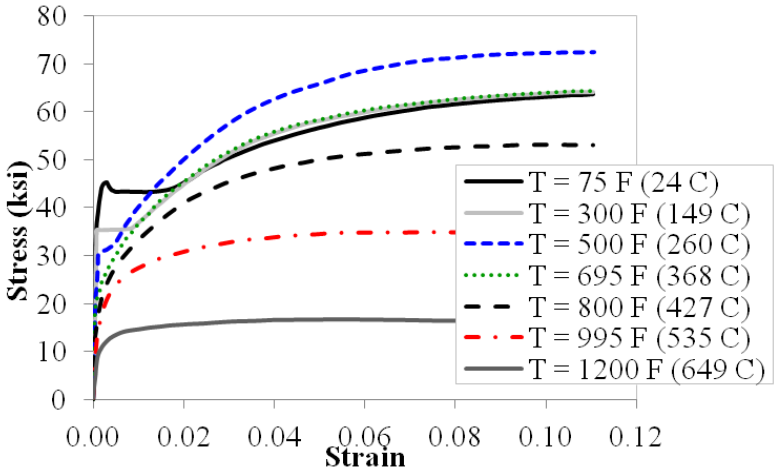

Figure 2.3. Stress-strain curves for ASTM A36 steel at elevated temperatures (adapted from Harmathy and Stanzak 1970).

Youssef and Moftah (2007) provided an overview of three different models for the yield strength of reinforcing steel at elevated temperatures. One of the models was from literature, and the other two were from Eurocode 2 (CEN 2004) and ASCE 78 Manual (ASCE 1992). The ASCE and literature models predict a gradual reduction in strength as the temperature increases from 20°C to approximately 800°C. In the Eurocode model, there is no reduction in strength for temperatures lower than 400°C, after which point there is a sharp drop in strength. All of the models predict that the steel has lost almost the entirety of its strength for temperatures exceeding 800° C.

Biondini and Nero (2011) developed finite element models of RC structures subjected to fire using the constitutive relationship for steel from the Eurocode 2. The Eurocode 2 provides the strength, Young's modulus, and strain (including stress-induced and temperature-induced) as a function of temperature. The temperature-induced strain is composed of thermal strain and creep strain. The creep strain is implicitly included in the EC2 equations. Biondini and Nero (2011) suggested that the implicit formulation is reasonably accurate for a structure that has low percentages of reinforcement or when the elevated temperature is not sustained for a long period of time. When using heat conduction to determine the spatial and temporal distribution of temperature in the RC structure, Biondini and Nero (2011) neglected changes in the thermal properties of steel at elevated temperatures. This is reasonably accurate because the reinforcing steel does not significantly affect the heat transfer in a reinforced concrete cross-section due to its small cross-sectional area in comparison with the cross-sectional area of concrete.

2.3 Models for Temperature Evolution during Fires

There are generally three approaches for evaluating the fire to which a structure may be exposed (Kodur 2008). The first (and simplest) approach is to use the tabulated data in the

building codes (e.g. Eurocode 2 (CEN 2004), ACI 216.1 (ACI and TMS 2014), or AS 3600 (Standards Australia Committee BD-002 2009)) that provide prescriptive requirements for providing structural fire protection. These requirements include minimum concrete cover, minimum reinforcement ratios, and minimum tie spacing. This method is based on experimental data and generally produces a conservative requirement for fire protection.

The second approach is to evaluate the structural performance under a standard fire scenario, such as ASTM E119 (ASTM 2014). This standard provides a temperature-time curve for a "standard" fire that is to be used for fire testing of structural components. This temperature-time curve is also used in analytical models to calculate the cross-sectional temperatures of a member as a function of time. The curve given in ASTM E119 starts at an ambient temperature of 68°F (20°C) at time 0, jumps to 1000°F (538°C) at t = 5 minutes, and then continues increasing until it reaches 2,300°F (1260°C) at t = 8 hours.

The third, and most complicated, approach is to generate a realistic fire scenario based on the details of the structure being analyzed. A realistic fire consists of a growth phase and a decay phase, and its characteristics are dependent upon the fuel load and ventilation (Kodur et al. 2009). Eurocode 1 (CEN 2002) provides calculation procedures for determining fire scenarios based on the fuel load and properties of the structure being analyzed. A comparison between the ASTM E119 curve and a sample parametric temperature curve developed using the procedures of Eurocode 1 is shown in Figure 2.4. Kodur et al. (2009) determined that fire resistance evaluated using the standard fire scenarios (e.g. ASTM E119) will usually be more conservative than fire resistance evaluated using a realistic fire scenario that has a decay phase.

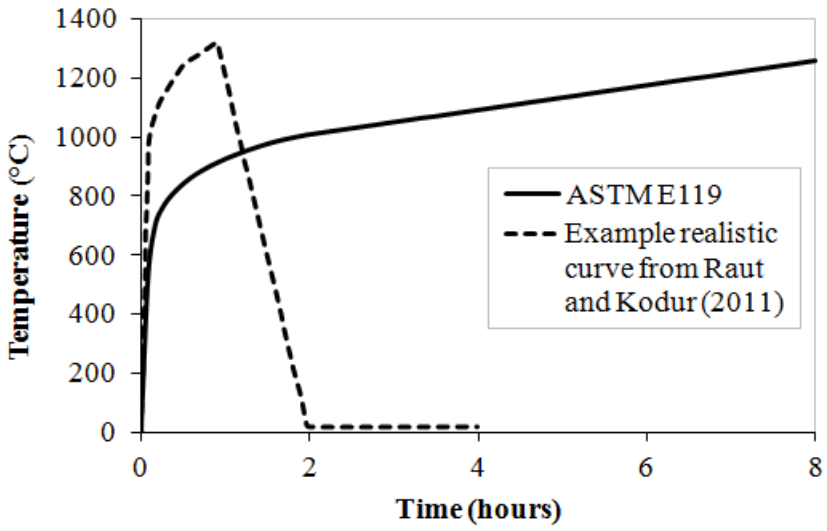

Figure 2.4. Comparison between standard fire curve (ASTM 2014) and natural fire curve (Raut and Kodur 2011).

2.4 Modeling Reinforced Concrete Behavior at Elevated Temperatures

Bamonte and Lo Monte (2015) determined that creep strain can usually be ignored for typical fire durations, but transient strain is a significant component of the total strain. Eurocode 2 implicitly takes into account the transient strain and the creep strain (as well as the creep strain in steel) by increasing the predicted total strain at elevated temperatures. Bamonte and Lo Monte compared four different models for concrete behavior under elevated temperature. They concluded that the Eurocode 2 models are the easiest to use and provide the closest match to experimental data. They also reported that second-order P-Δ effects have a strong influence on fire rating due to increased concrete deformability under elevated temperatures. Therefore, the predicted concrete modulus of elasticity is an important property that has a significant effect on time to failure.

Youssef et al. (2008) provided a comprehensive overview of concrete properties at three stages: elevated temperature, during cooling, and post-cooling. They proposed models from

literature for the following properties at each of these stages in the fire process: concrete compressive strength, concrete tensile strength, strain at peak compressive stress, modulus of elasticity of concrete, yield strength of reinforcing, bond strength of reinforcing, and the stress-strain relationship for concrete. The models for the elevated temperature properties can be used for fire modeling of reinforced concrete structures. The cooling and post-cooling properties are important for long-term assessment of RC structures that were subjected to fire. Youssef et al. (2008) determined that some properties show recovery during the post-cooling stage (such as compressive strength and modulus of elasticity) due to rehydration of the concrete.

Dwaikat and Kodur (2008) performed an analytical comparison of fire predictions for a reinforced concrete beam using three codes documents, i.e. Eurocode 2, ACI 216.1, and AS 3600, and from a macroscopic finite element (FE) model. In the macroscopic FE model, sectional analysis is performed at several locations along the length of a member, and the section responses are used to predict the total response of the member. Dwaikat and Kodur determined that Eurocode 2 prescriptive requirements result in the most conservative predictions, and that ACI 216.1 models may not be conservative in some cases (simply supported beam in this study). Additionally, the failure of a concrete element is dependent on several failure criteria, such as temperature of the reinforcing, strength, deflection, and rate of deflection.

A case study by Rini and Lamont (2008) illustrated the possibilities of using advanced finite element models in ABAQUS (2006) to analyze a structure under a realistic fire scenario and design the fire protection accordingly. The case study consisted of an analysis of Ropemaker Place, a 21-story steel-framed office building in London, subjected to a realistic fire on a portion of one floor plate. The fire curve was developed based on the Eurocode 1 (CEN 2002) provisions for parametric fire curves. The initial design for the structure was analyzed in ABAQUS (2006)

to determine the fire performance. Based on the response, the level of fire resistance was increased or decreased as necessary to meet performance criteria, and then the structure was reanalyzed. This iterative procedure was continued until all performance criteria were met. One advantage of this type of analysis is that the fire protection can be optimized according to the particular strengths and weaknesses of the whole-building behavior during fire, which leads to cost savings for the building owner (Rini and Lamont 2008). For example, fire proofing on some of the secondary beams was removed, and the reinforcement in the slab was increased to reduce cracking and thereby improve compartmentalization performance. The researchers also detailed the connections to allow for behavior that is more ductile during the thermal expansion and contraction seen in fire scenarios. In contrast, fire protection using prescriptive approaches applies somewhat generic requirements to every structural component, regardless of changes in capacity due to structural-level behavior. The performance-based approach allowed the researchers to meet specific performance criteria, namely stability throughout fire and limiting spread of fire through effective compartmentalization, based on a realistic estimate of the building performance. Despite the large deflections observed in the structure—up to 1.3 m in the floor system for a span of 13.5 m and lateral deflections up to 15 mm in columns—stability was maintained throughout the analysis due to tensile membrane action and load redistribution, as shown in Figure 2.5.

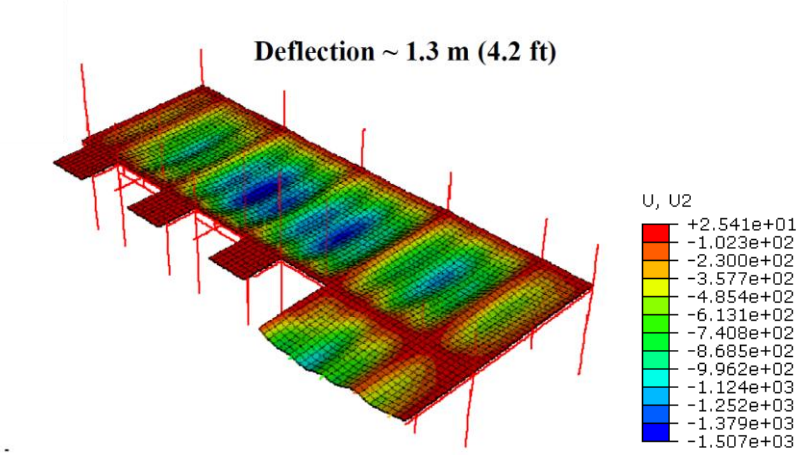

Figure 2.5. Deflection contour plot of floor slab post-fire from Ropemaker Place case study. Rini, D., and Lamont, S. (2008). "Performance based structural fire engineering for modern building design." *Proc., 2008 Structures Congress*. Used under fair use, 2015.

The performance-based approach has also been demonstrated through a case study of a multi-story transit center that uses external steel braced frames as part of the architectural design (Rini et al. 2011). The performance-based methods allowed the satisfaction of architectural requirements on the building façade by eliminating the need for external fire proofing on the exposed braces. Despite their use in various studies, finite element models are computationally expensive and are only appropriate for large, specialized projects in which such analysis may be justified. Additionally, the extension of refined finite element models to analyses for combined earthquake and fire effects may not be feasible. The constitutive models would likely need to be modified to incorporate cyclic behavior, and the computational time would certainly increase, potentially by an amount that renders parametric analyses impossible.

2.5 Performance-Based Design and Building System Behavior at Elevated Temperatures

In recent years, there has been an increased focus on performance-based design methods for fire engineering. In comparison to prescriptive, conservative design methods that do not take

into account specific beneficial building characteristics (such as ventilation, layout, and fuel load), performance-based design methods may lead to relaxed requirements for fire protection, resulting in economic and aesthetic benefits. There are several levels of detail possible for an analysis, including extent of model (component, substructure, or whole building) and type of fire curve (i.e. based on a standard fire curve or on a realistic fire scenario). A single-component analysis is conceptually simple and easy to validate with existing test data, but it cannot take into account system-level behavior, such as restraint of ends or membrane behavior. Conversely, a substructure or whole-building analysis is more realistic, but can be computationally demanding and impractical for typical building design. Fire curves established in code standards (e.g. ASTM E119 (ASTM 2014)) are easy to implement but not realistic since they do not include the temperature decay periods. In comparison, realistic fire curves more accurately describe the temporal evolution of temperature, but they require detailed calculations based on information about ventilation, layout, and fuel load.

The typical process for performance-based design consists of three phases. The first phase includes the selection and establishment of the fire (temperature-time) curve. A standard fire curve may be used, or a realistic fire curve may be developed using acceptable calculation methods, such as those outlined in Eurocode 1 (CEN 2002). The second phase includes a heat conduction analysis to determine the spatial distribution of temperature in the structure as a function of time. Methods for doing this, ranging from simpler to more refined, include: i) using prescriptive cover requirements to ensure a critical temperature is not reached in the member (e.g., *International Building Code* 2015); ii) using temperature distribution graphs that provide cross-sectional temperature for standard structural shapes under the ASTM E119 fire exposure (examples are provided in Phan et al. 2010); iii) implementing a time-dependent heat conduction

analysis using the finite element method. The third phase includes a structural analysis based on the elevated-temperature mechanical properties of the member materials. The structural analysis should take into account load capacity, deflection criteria, and compartmentalization requirements.

Performance-based design guidelines are gradually being incorporated in building codes. European standards moved towards a performance-based approach with the fire provisions in the Eurocodes. Eurocode 1 provides guidelines for establishing realistic fire curves, and Eurocode 2 provides material properties at elevated temperatures for several types of concrete and reinforcing steel. The U.S. building codes are generally still prescriptive in nature, but steps have been made to make room for performance-based design. The ASCE 114 document (Parkinson et al. 2008) provides guidelines for thermal analysis of steel sections to determine required fire protection for limiting the steel temperature to acceptable values. Appendix 4 in the AISC Steel Design Manual (*Steel Construction Manual* 2011) provides several options for performance-based design of steel structures and includes elevated-temperature properties of structural steel. The ACI 216 document (ACI and TMS 2014) provides guidance on prescriptive concrete cover requirements and methods for calculating fire resistance times for standard concrete elements. U.S. design guidelines are more advanced for steel construction than for concrete construction. The NIST Technical Note 1681 (Phan et al. 2010) provides a detailed overview of the state-of-the-practice in performance-based fire engineering for concrete and steel structures.

The Cardington tests at the Building Research Establishment (BRE) Laboratories in Cardington, UK encompassed full-scale fire testing of an 8-story steel-framed composite structure, a 7-story reinforced concrete structure, and a 6-story timber-framed structure (Wang et al. 2013a). The reinforced concrete structure was intended to be similar to a standard office

building designed according to the Eurocodes. The Cardington tests revealed the need to consider important structural behavior that cannot be adequately captured through component-level fire analysis or testing. Specifically, the reinforced concrete structure exhibited compressive membrane behavior in the floor slabs, extensive spalling of the slab, and significant horizontal displacement of the concrete columns due to thermal expansion of the floor slab (Chana and Price 2003). During the testing, the fire was contained in a compartment on the first floor. As the temperature of the concrete slab increased, its thermal expansion was resisted by the concrete in surrounding compartments that was not subjected to fire effects, causing horizontal compression in the heated slab. This compression allowed the slab to transfer its loads to the supporting columns through diagonal compression membranes (Figure 2.6). Spalling of the heated underside of the slab was also observed, exposing reinforcement and allowing some of the reinforcement to separate from the concrete, but the slab continued to carry loads throughout the duration of the fire testing. The average measured outward displacement of the external columns due to the thermal expansion of the slab was approximately 33 mm, with a maximum column displacement of 67 mm and a minimum of 20 mm (Bailey 2002). The columns continued to carry loads throughout the duration of the fire testing.

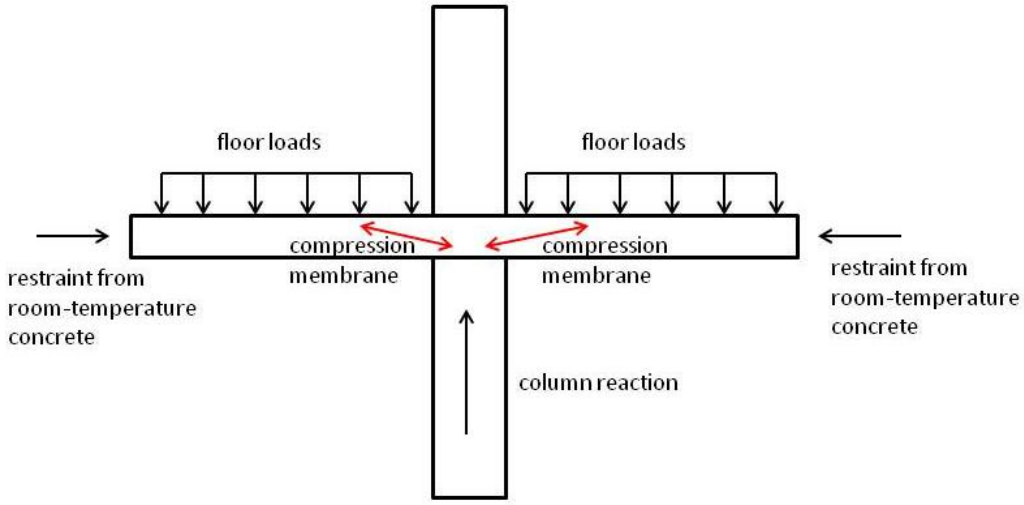

Figure 2.6. Compression membrane in concrete slab during Cardington tests, adapted from Chana and Price (2003).

The full-scale testing at Cardington revealed the importance of understanding the system-level behavior of a reinforced concrete building in fire. While exposed reinforcement and large displacements may have indicated failure in a member-level test, the system-level testing revealed that the structure could maintain stability throughout a fire through system-level mechanisms, such as compression membranes. Conversely, system-level interactions between members have the potential for adverse effects. For example, the restraint provided by the columns can be beneficial for the slabs (compression membrane behavior), but the outward displacement of the columns can cause reduced column capacity and second-order P-Δ effects that can cause instability. Additional research and analytical tools are needed for a more complete understanding of system-level behavior.

2.6 Earthquake-fire Interaction

Current building codes require designers to consider the effects of earthquake damage and the effects of fire damage, but the effects are considered separately (Behnam and Ronagh

2014a). In reality, fire in buildings can occur after serious earthquakes because of damaged infrastructure, such as gas lines and electrical wires. In addition, fire suppression is hindered in a post-earthquake fire due to overburdened emergency response personnel and damages to sprinkler systems and water distribution systems used for fire suppression. Historically, post-earthquake fires caused significant damage in the 1906 San Francisco earthquake, the 1923 Tokyo earthquake, and the 1995 Kobe, Japan earthquake (Mousavi et al. 2008). In the case of a post-earthquake fire, a building must be able to withstand compound damage due to both the earthquake and the fire. New structural models must be developed to analyze damage to structures due to post-earthquake fires. Currently, programs are available that are specifically developed for analyzing structures in fire (such as SAFIR and VULCAN), and finite element analysis (FEA) programs are available that can perform earthquake or fire analysis individually (such as ANSYS or ABAQUS), but there are no programs available for the direct analysis of a coupled earthquake-fire scenario (Mousavi et al. 2008). Additionally, previous studies have pointed out that FEA programs are computationally expensive and may not allow performance-based structural design and assessment. Efficient models for analysis of combined earthquake and post-earthquake fires are deemed necessary to establish new building code standards and to evaluate the safety of structures in a multi-hazard environment.

Few experimental studies have been performed to study structural performance during combined earthquake and post-earthquake fire scenarios. Bhargava et al. (2012) experimentally examined the performance of a reinforced concrete frame subjected to earthquake motion, followed by fire damage. The earthquake damage was simulated through quasi-static cyclic loading using a reaction wall. The fire test lasted for one hour, and the peak concrete surface temperature of a column, as recorded by thermocouples, was 1000°C. Their testing of the 3 m

tall frame showed that the post-earthquake residual displacement of 19 mm was reduced to 12 mm after the fire test. Additionally, the autogenous thermal expansion affected the final shape of the frame, and damage to the frame was noted through significant spalling, exposed rebar, and cracking. Images of the frame before, during, and after the fire testing can be seen in Figure 2.7. Given the limitations of experimental equipment, analytical model-based simulation is deemed necessary to investigate the impact of post-earthquake fires on multi-story prototype RC buildings.

Figure 2.7. Reinforced concrete frame subjected to fire testing after earthquake damage. Bhargava, P., Kamath, P., Usmani, A., May, I., B Singh, B., Gillie, M., Sharma, U. K., Kumar, V., Pankaj, P., Torero, J., Y Singh, Y., and Zhang, J. (2012). "Full-scale testing of a damaged reinforced concrete frame in fire." *Proceedings of the ICE - Structures and Buildings*, 165, 335–346. Used under fair use, 2015.

There have been limited efforts to assess analytically the performance of structures under combined earthquake and fire effects. Behnam and Ronagh (2014a) performed a finite element analysis of a reinforced concrete frame subjected to earthquake damage (modeled using SAP),

followed by fire damage, which was simulated with several different fire curves using the program SAFIR. They also compared the structural performance with that of an RC frame that was exposed to fire alone. The frame analyzed was a two-bay, three-story reinforced concrete structure with a story height of 3.3 m. They determined that the structure did not exhibit failure when subjected to fire, but that the structure did incur severe damage when subjected to both earthquake and fire effects, as shown in Figure 2.8. In several of the combined earthquake and fire scenarios, local failure modes occurred when beam deflections became unstable, and global failure modes occurred when column deflections became unstable and caused instability of the structure. The obtained damage pattern was dependent on the fire curve used and the areas where the fire was applied (first floor, multiple floors, etc.). The method employed by Behnam and Ronagh (2014a) was overly complicated, however, as it requires the user to utilize two analysis programs and to define the extent of plastic damage due to the earthquake loads prior to performing the fire analysis. The level of cracking and spalling in the concrete must be estimated using descriptive definitions in FEMA 356, which is imprecise and may not accurately reflect the conditions in the structure being analyzed. Additionally, the constitutive law for concrete at elevated temperatures was described using the Eurocode equations. The Eurocode equations implicitly account for transient and creep strains, which may not accurately account for different stress levels and fire durations.

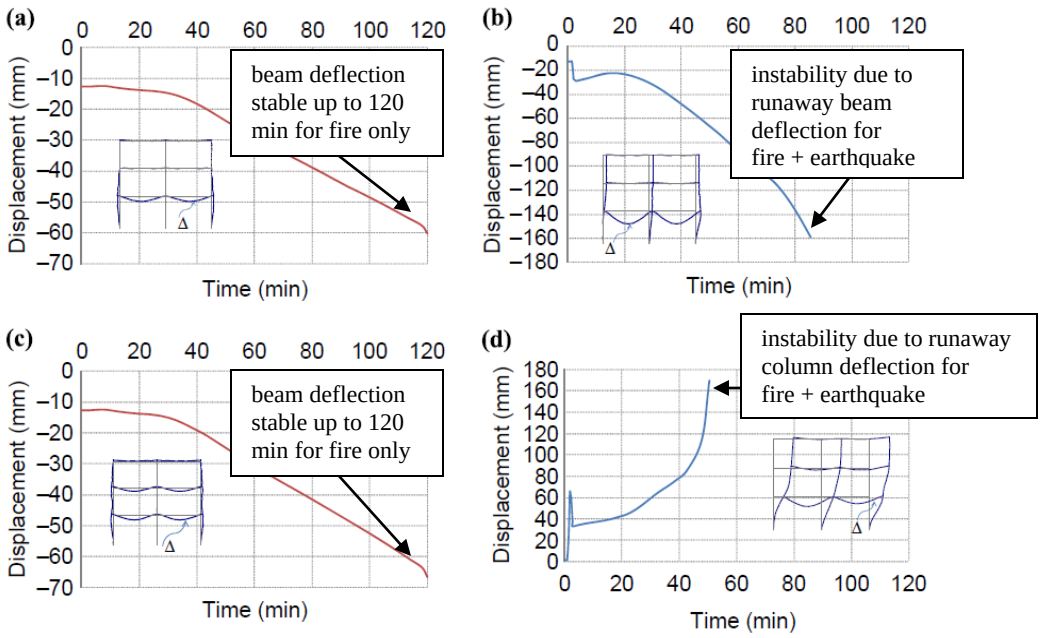

Figure 2.8. Displacement time histories for (a) frame subjected to fire damage on 1st floor, (b) frame subjected to earthquake + fire damage on 1st floor, (c) frame subjected to fire damage on 1st and 2nd floors, and (d) frame subjected to earthquake + fire damage on 1st and 2nd floors. Behnam, B., and Ronagh, H. (2014a). "A study on the effect of sequential post-earthquake fire on the performance of reinforced concrete structures." *International Journal of Structural Integrity*, 5(2), 141–166. Used under fair use, 2015.

In an effort to investigate potential design methods, Behnam and Ronagh (2014b) also performed a numerical study of a five-story reinforced concrete frame under the effects of a post-earthquake fire. In this study, the earthquake damage was simulated using a pushover analysis in SAP2000, where the frame was subjected to displacements that correspond to the limits for the Immediate Occupancy level (i.e. maximum drift of 1%) in FEMA 356. The pushover analysis results were then input into the program SAFIR, which uses fiber elements to simulate the damage due to fire. In a fiber element, several cross-sections along the length of the element are discretized into "fibers." Each fiber follows a uniaxial stress-strain law, and integration over the fibers is performed to determine the distribution of stress and strain on the entire cross-section. Behnam and Ronagh (2014b) recommend the use of a post-earthquake fire (PEF) factor that

would increase the specified base shear so that the structure would remain in the IO level after a PEF. An iterative process was used to incrementally increase the base shear and redesign the structure until the specified performance level was met at the end of the numerical analysis. In their case study, the PEF factor for the five-story structure subjected to a fire with a duration of 2.5 hours was 1.11. Once the PEF factor is determined, it is straightforward to incorporate it into traditional earthquake design, but the methods for obtaining the factor require much iteration and redesign of the structure. The time required for this type of analysis would prohibit extensive parametric studies, which are necessary for developing design guidelines. Additionally, the constitutive laws used are based on the Eurocode equations for elevated temperature behavior, which are not always accurate due to the implicit inclusion of transient and creep strains in concrete. Improved methods for analysis and design are needed in order to move forward with performance-based design.

2.7 Simulation Tools for RC Structures under Earthquake Loading

A variety of analytical methods have been developed and used for the simulation of reinforced concrete (RC) components and systems under cyclic mechanical loading, such as earthquakes. The simplest models are based on nonlinear beam elements, but they cannot accurately capture the axial-shear-flexure interaction effect, which is important for RC walls. Additionally, beam models are based on the assumption that plane sections remain plane, which may not be appropriate for some regions, such as beam-to-column joints in RC frames. Finite element methods have also been developed and successfully used for the analysis of RC construction under cyclic loading (e.g., Koutromanos 2011). Finite element models are conceptually complicated, including many parameters that cannot be readily calibrated from material test data. Furthermore, nonlinear finite element models are computationally demanding:

a parametric analysis on a single structural component, such as an RC wall, may require the use of a supercomputer to ensure completion within a reasonable amount of time.

Nonlinear truss methods have been developed to model cyclic mechanical loading of RC structures. In truss methods, reinforced concrete is modeled through the use of vertical and horizontal concrete and steel truss elements, as well as diagonal unreinforced concrete truss elements. The truss method has the advantage that uniaxial constitutive laws, which are simpler and more readily available from test data than multi-axial constitutive laws, are used for the truss elements. Additionally, the truss method naturally captures the interaction of axial, shear, and flexural forces in an RC wall. Truss models are also conceptually simpler and computationally more efficient than refined finite element models, allowing for extensive parametric analysis.

Panagiotou et al. (2012) developed a nonlinear truss model for reinforced concrete walls subjected to cyclic loading (e.g. earthquakes). To implement the model, a reinforced concrete wall is subdivided into vertical, horizontal, and diagonal concrete and steel truss elements. The vertical elements represent the vertical steel reinforcement and the cross-sectional area of the surrounding concrete. Similarly, the horizontal elements represent the reinforcement and surrounding concrete in the horizontal direction. The diagonal unreinforced elements represent diagonal compression struts that develop when the wall is subjected to horizontal shear loads. The shear loads cause a state of shear stress on the horizontal and vertical planes of material, which results in principal compressive and tensile stresses on the diagonal planes (Figure 2.9). The diagonal concrete elements account for this stress, as it is not accounted for through the horizontal and vertical truss elements. For the diagonal elements, the effects of transverse tensile strain are taken into account through the use of transverse strain elements with zero stiffness, which act as simulated strain gauges. For concrete that is in a biaxial stress state, tension in one

direction will cause a reduction in compressive strength in the transverse direction. To capture this effect, if the concrete in the diagonal elements is subjected to transverse tensile strain (as measured using the strain gauge elements), then the compressive stress is multiplied by a reduction factor, β. The reduction factor varies with the magnitude of tensile strain, causing a larger strength reduction factor for larger tensile strains. This truss model was validated using experimental research for walls that are dominated by flexure-shear interaction (FSI).

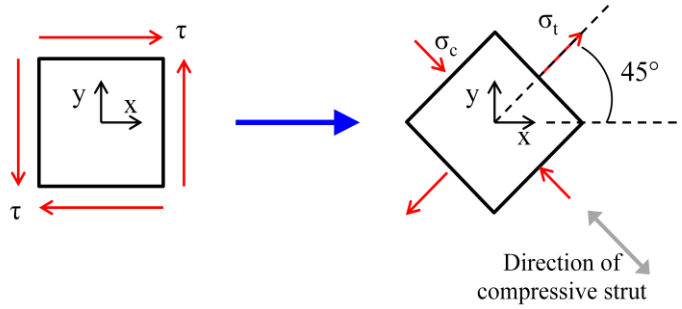

Figure 2.9. Compressive strut in concrete under shear loading.

Moharrami et al. (2014) extended the truss model from Panagiotou et al. (2012) to apply it to shear-dominated reinforced concrete columns, as illustrated in Figure 2.10. The constitutive laws were enhanced to account for the aggregate interlock contribution to the shear resistance of the column. Moharrami et al. (2014) also proposed a method for calculating the inclination angle of the diagonal concrete elements based on the applied loads and material strengths of the column. Strain penetration was incorporated into this model by using strain penetration elements that are rigid in compression and produce the required slip upon yielding in tension. This truss model was validated using experimental results from both quasi-static and dynamic testing. Figure 2.10 illustrates the capability of the model to predict the level and location of damage in an RC column.

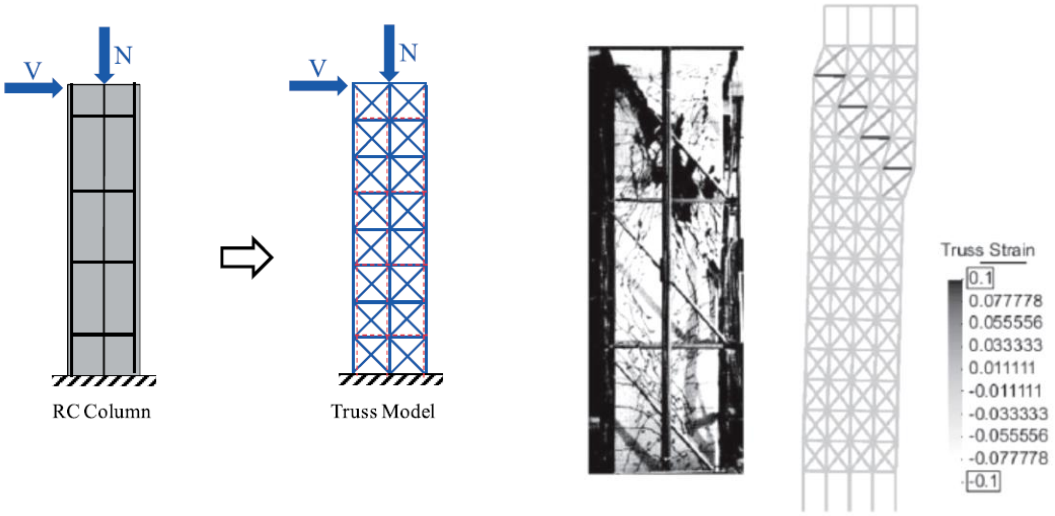

(a) (b)

Figure 2.10. (a) nonlinear truss model for modeling a reinforced concrete column. (b) damage in RC column observed in experiment and predicted by truss model (deformations in prediction magnified by a factor of 5).
Moharrami, M., Koutromanos, I., Panagiotou, M., and Girgin, S. C. (2014). "Analysis of shear-dominated RC columns using the nonlinear truss analogy." *Earthquake Engineering & Structural Dynamics*. Used with permission.

3 Analysis Methodology

3.1 Introduction

Current building codes require consideration of earthquake and fire effects separately, but they do not account for the combined effects during a post-earthquake fire. Historically, damage to infrastructure during earthquakes can initiate building fires and cause significant structural damage. Design guidelines for combined earthquake and fire effects are needed to protect against this hazard, but the structural analysis tools that are currently available are inadequate for developing these guidelines. The current tools either cannot account for the combined effects, or they are too computationally expensive. Additionally, many of the currently available tools do not explicitly take into account transient strain. Because transient strain can be a significant portion of the total strain in concrete at elevated temperatures (Anderberg and Thelandersson 1976), implicitly including it can lead to inaccuracies in the analysis. A new method is needed that can accurately analyze a structure subjected to combined earthquake and fire effects and that is computationally efficient to aid in the development of design guidelines.

The aim of this study is to modify an existing nonlinear truss model for reinforced concrete structures so that it can account for the effects of elevated temperatures during fires. The existing truss model has already been validated for predicting earthquake performance (Moharrami et al. 2014; Panagiotou et al. 2012), and extending it to incorporate temperature affects allows the model to be used to study RC structural performance during combined earthquake and fire scenarios.

3.2 Existing Nonlinear Truss Model for RC Structures

The present research is based upon the nonlinear truss method for reinforced concrete that has been presented by Panagiotou et al. (2012) and Moharrami et al. (2014). This method is used for the modeling of cyclic behavior of reinforced concrete shear walls and columns. The behavior of these structural elements is difficult to model due to the nonlinearities that arise from the interaction between axial, shear, and flexural forces on the members (Panagiotou et al. 2012). The nonlinear truss model has the following advantages over other methods of modeling reinforced concrete columns and shear walls. First, the nonlinear truss model is conceptually simple and based on material-level behavior. Beam-based modeling methods require the addition of nonlinear springs to capture the deformation and strength degradation due to shear damage, and these springs must be calibrated using experimental data and manual adjustment (Moharrami et al. 2014). Second, the nonlinear truss model is based on uniaxial constitutive laws for concrete and steel. In the case of nonlinear finite element models, multi-dimensional constitutive laws must be defined, and the models require significant computational power. Conversely, uniaxial stress-strain laws required in the nonlinear truss method are more readily available in literature, especially with regards to cyclic loading (for earthquake analysis) and elevated temperature behavior (for fire analysis). The computational power required by the nonlinear truss method is significantly reduced compared to nonlinear finite element models. For these reasons, the nonlinear truss method was deemed to be the optimal choice for modeling combined earthquake and fire effects in reinforced concrete. In the present study, the truss analogy was implemented in Finite Element Analysis Program (FEAP – Taylor 2013). FEAP allows the user to define new material constitutive laws and solution algorithms, so it is well suited for research applications.

3.2.1 Existing Constitutive Relationships in the Nonlinear Truss Model

The concrete elements in the present study used a stress-strain law developed by Koutromanos (2011), as illustrated in Figure 3.1. The concrete in compression is linear-elastic up to a stress of f_0 and reaches a peak stress of f'_c at a strain of ε_1, at which point softening occurs. The initial softening curve is described by a parabolic function, and the remainder of the softening curve is a linear function. Upon reaching the ultimate strain at ε_u, the concrete has a residual strength that is specified as a proportion of the compressive strength. Concrete in tension is linear elastic up to a tensile strength of f_t at a strain of ε_{ini}. Larger tensile strains result in exponential softening. This concrete constitutive law can also take into account the effects of transverse strain on the compressive strength, in accordance with the modified compressive field theory (Vecchio and Collins 1986). Concrete that is in a biaxial stress state exhibits lower compressive strength if the transverse strain is tensile. This effect is accounted for in the diagonal concrete truss elements using a reduction term, β. The β term is multiplied by the concrete compressive stress to account for the reduction in strength. An additional two nodes are defined for each diagonal truss element to be used as a strain gauge with zero stiffness that is perpendicular (or nearly perpendicular) to the truss element. The displacements of these two nodes allow for the calculation of the transverse strain. The β term is a function of this transverse tensile strain, ε_t. In the present study, the dependence of β on ε_t is based on a tri-linear curve, shown in Figure 3.1b, where $\beta_1 = 0.3$, $\beta_2 = 0.1$, $\varepsilon_{t1} = 0.01$, $\varepsilon_{t2} = 0.025$. For the vertical and horizontal concrete elements, transverse strain is not taken into account and $\beta = 1$.

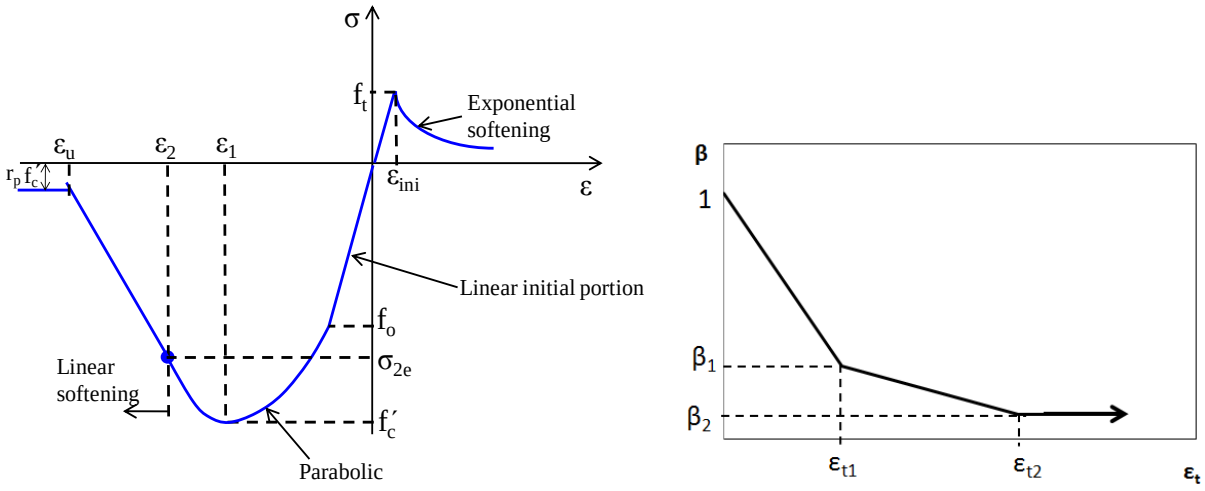

Figure 3.1. (a) Constitutive Relationship for Concrete (Koutromanos 2011) and (b) Variation of transverse tension reduction factor, β.
Koutromanos, I. (2011). "Numerical Analysis of Masonry-Infilled Reinforced Concrete Frames Subjected to Seismic Loads and Experimental Evaluation of Retrofit Techniques." University of California, San Diego. Used under fair use, 2015.

The steel constitutive law that is used in this research is the one proposed by Kim (2014). This formulation is an enhanced version of the Dodd and Restrepo (1995) model, but it uses a non-uniform rational B-spline interpolation for the nonlinear portions of the hysteretic behavior. Using this interpolation allows the stress to be calculated explicitly, which is more computationally efficient than the iterative method used by Dodd and Restrepo (Kim 2014). The steel stress-strain law is linear elastic in compression and tension until it reaches the yield point, f_y, at a strain of ε_y. The stress-strain law includes strain hardening, the onset of which occurs at strain ε_{sh}. The steel reaches an ultimate stress of f_{su} at a strain of ε_{su}. This model can also incorporate buckling and fatigue rupture, but those capabilities are not utilized in the present study.

3.2.2 Truss Method Verification and Validation

To verify the implementation of the truss method in FEAP, two of the case studies from Panagiotou et al. (2012) were analyzed. The first case study was based on experimental testing of an RC shear wall that was subjected to lateral displacements at the top of the wall (Sittipunt et al. 2001). There was no axial load on the wall, and the top of the wall was free to rotate. The truss structure modeled in FEAP is shown in Figure 3.2, and the obtained hysteretic curves are compared to those obtained by Sittipunt et al. (2001) in Figure 3.3. The circular markers on the graphs represent the point at which softening occurs in the diagonal concrete elements (i.e. the strain in the concrete element is larger than the strain at peak compressive stress), and the square markers represent the point at which crushing occurs in the diagonal concrete elements (i.e. the strain in the concrete element is larger than the ultimate strain). In the experimental test, the wall failed at a drift ratio of 1.4% due to web crushing (Sittipunt et al. 2001). The model of Panagiotou et al. (2012) exhibited softening at a drift ratio of 1.3% and crushing at a drift ratio of 2.5%. The corresponding drift ratios in the FEAP analysis are 1.36% and 1.37%, respectively. In the experimental testing, the strength of the truss was measured as 614 kN. The FEAP model predicted the strength of the truss as 544 kN, which is underestimated by about 11%. The truss model in the FEAP analysis includes bond slip elements at the base of the wall. These elements account for the slip between the reinforcement and the concrete base of the structure (the so-called strain penetration effect discussed in Moharrami et al. 2014), which affects the displacement response of flexure-dominated walls and columns due to increased rotational compliance at the base. These bond slip elements are modeled in accordance with the method used in Moharrami et al. (2014).

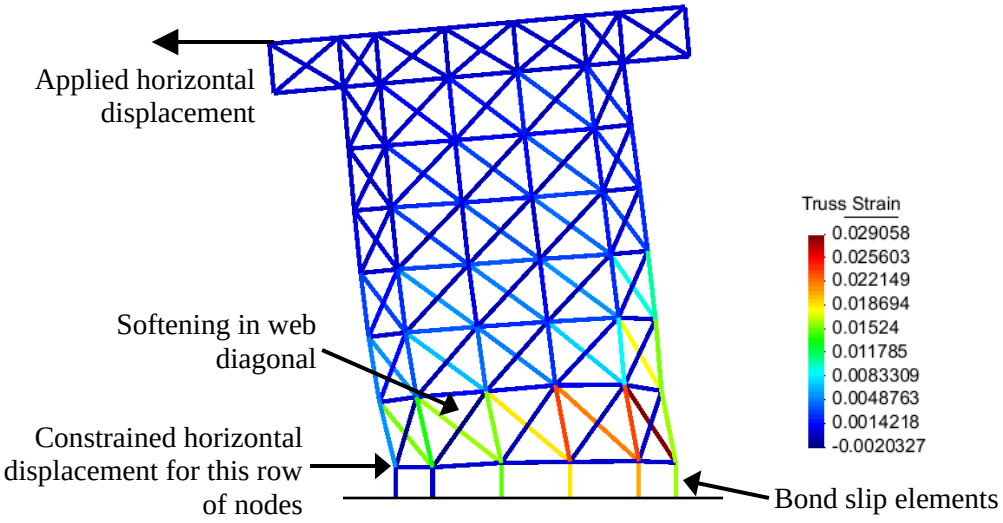

Figure 3.2. Truss structure based on experimental work by Sittipunt et al. (2001) with strain contours plotted at time of softening in web diagonal (deformation magnified by a factor of 10).

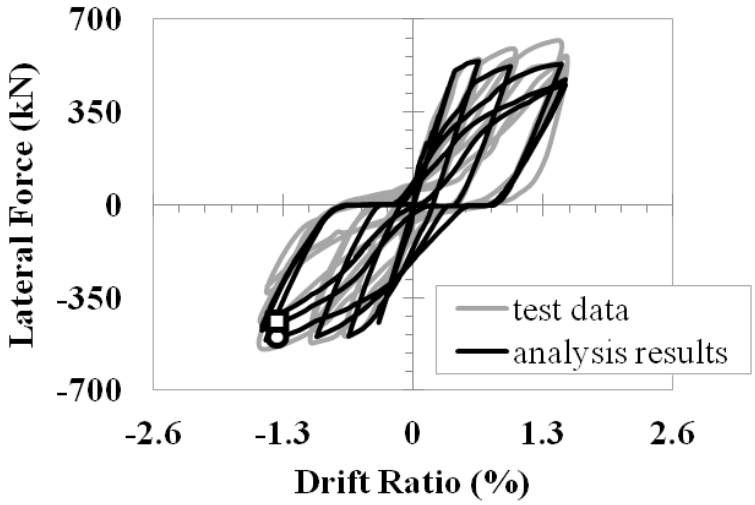

Figure 3.3. Comparison of analysis results from FEAP model with test data from Sittipunt et al. (2001). Circle indicates softening, and square indicates crushing of diagonal concrete.

The second case study was based on the experimental testing of a RC shear wall that had restrained rotation at the top and an axial load ratio of 5% (Massone Sanchez 2006). The truss structure as modeled in FEAP is shown in Figure 3.4, and the response curves from the test data

and the FEAP analysis are presented in Figure 3.5. As shown in Figure 3.4, softening in the bottom concrete diagonal member causes opening of tensile cracks in the concrete, which is illustrated by the variation in displacements above and below the cracking. Prior to softening, the shear is carried through the diagonal compressive strut that forms (Figure 3.4a), but after softening the shear must be carried through the horizontal steel members that cross the crack (Figure 3.4b). Diagonal crushing of the concrete in the experimental work was observed at a drift ratio of 0.8% (Massone Sanchez 2006). The Panagiotou et al. truss model exhibited softening at a drift ratio of 0.72% and exhibited crushing at a drift ratio of 0.86%. The FEAP analysis predicted softening at 0.71% and predicted crushing at a drift ratio of 0.77%. In the experimental testing, the strength of the truss was measured as 654 kN. The FEAP model predicted the strength of the truss as 763 kN, which is overestimated by about 17%. One modification that could improve the agreement between predicted and observed strength is to adjustment the β-factor curve so that the transverse tensile strain has a more severe effect on the compressive strength of the diagonals. Additionally, improvement may be obtained by refining the concrete constitutive law in the FEAP model so that it more closely matches the experimentally measured stress-strain curve.

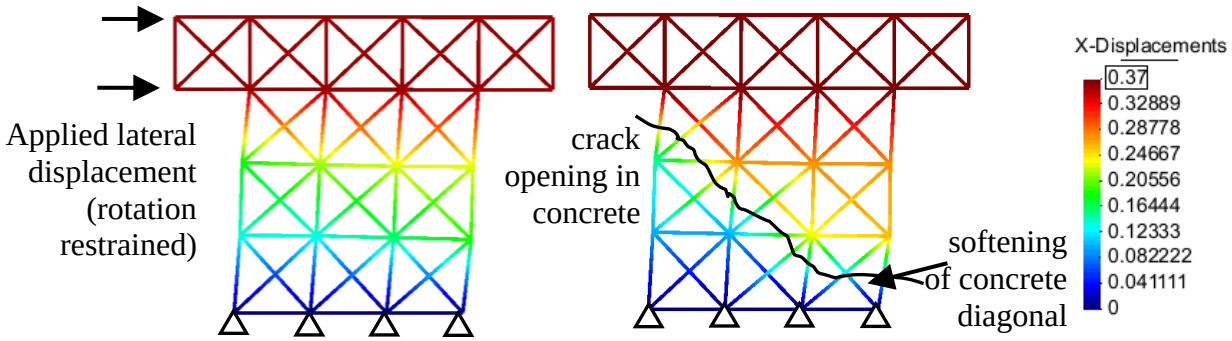

Figure 3.4. Truss structure based on experimental work by Massone Sanchez (2006) with displacement contours: prior to softening of diagonal concrete (a), and after softening of diagonal concrete (b). Deformation magnified by a factor of 10.

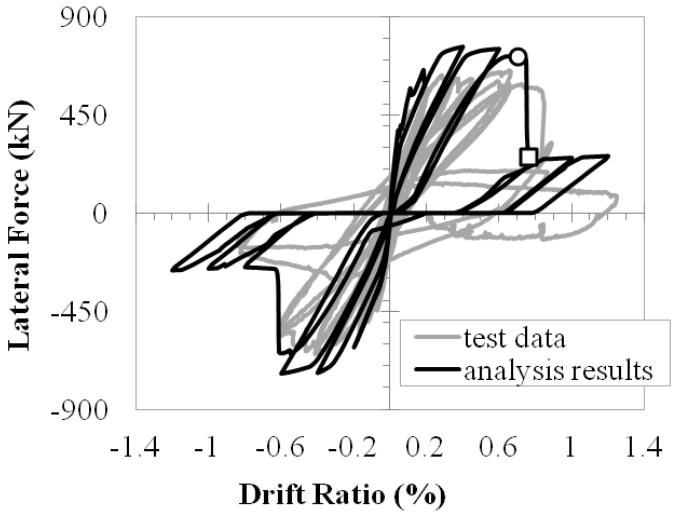

Figure 3.5. Comparison of analysis results from FEAP model with test data from Massone Sanchez (2006). Circle indicates softening, and square indicates crushing of diagonal concrete.

3.3 Enhancement of Material Models to Account for Effect of Elevated Temperature

As described in Chapter 2, elevated temperatures, such as those developing due to fire, can significantly affect the behavior of concrete. The compressive strength of the material reduces, while autogenous (i.e. stress-free) thermal strains and strains due to chemical reactions also occur. Similar effects are observed in the reinforcing steel. Additionally, the thermal conductivity and specific heat of concrete change under elevated temperatures. In order to represent these effects in the existing nonlinear truss model, the dependence of the mechanical and thermal properties of concrete on temperature must be mathematically described. Several design documents, such as the Eurocode 2 (CEN 2004), the ASCE 78 Manual (ASCE 1992), and the ACI 216.1 document (ACI and TMS 2014), provide models for concrete and reinforcing steel under elevated temperatures. Extensive experimental and analytical research has also been performed to determine the behavior of concrete under elevated temperatures, including

Anderberg and Thelandersson (1976), Li and Purkiss (2005), Youssef and Moftah (2007), and Knaack et al. (2009). It should be noted that experimental testing is usually performed on concrete specimens soon after casting (common age is 28 days), so the material models derived from these tests may not capture the behavior of old structures under fire effects. Still, these models can be used as a first approximation, especially given the absence of pertinent experimental data.

The proposed models for reinforced concrete under elevated temperatures vary in complexity, ease of implementation, and testing methods they are based upon. The present study aims to establish material models that allow straightforward implementation while still capturing the salient features of material behavior. For this reason, the Eurocode 2 (EC2) equations were used for several of the concrete and reinforcing steel properties at elevated temperatures. The EC2 equations have been well documented in research, and they are relatively simple expressions that depend on temperature. However, the EC2 equations for concrete do not explicitly account for the transient and creep strains, but rather implicitly account for these strains by increasing the ultimate strain at elevated temperatures. Implicitly including the temperature-dependent strains in the nonlinear truss analysis would require modifications in the shape of the stress-strain curve, which could cause problems with the constitutive laws. For these reasons, equations from literature were used to describe the stress-strain behavior of the concrete at elevated temperatures, as detailed below.

3.3.1 Material Models: Effect of Elevated Temperature on Thermal Properties

This section presents the material models used to describe the thermal properties of concrete at elevated temperatures. The thermal properties are required for a heat transfer analysis of a concrete structure, and they include the density, specific heat, and thermal conductivity.

The variation of the density of concrete with temperature is described by the following equations, which are proposed in EC 2 (CEN 2004).

$\rho(T) = \rho_0$ for $20°C \leq T \leq 115°C$ (Eq 3.1)

$\rho(T) = \rho_0 \cdot (1-0.02(T-115)/85)$ for $115°C \leq T \leq 200°C$ (Eq 3.2)

$\rho(T) = \rho_0 \cdot (0.98-0.03(T-200)/200)$ for $200°C \leq T \leq 400°C$ (Eq 3.3)

$\rho(T) = \rho_0 \cdot (0.95-0.07(T-400)/800)$ for $400°C \leq T \leq 1200°C$ (Eq 3.4)

where ρ_0 is the density at T = 20 °C.

The EC 2 (CEN 2004) also establishes the following expressions, describing the variation of specific heat as a function of temperature.

$c_p(T) = 900$ J/(kg K) for $20°C \leq T \leq 100°C$ (Eq 3.5)

$c_p(T) = 900 + (T - 100)$ J/(kg K) for $100°C \leq T \leq 200°C$ (Eq 3.6)

$c_p(T) = 1000 + (T - 200)/2$ J/(kg K) for $200°C \leq T \leq 400°C$ (Eq 3.7)

$c_p(T) = 1100$ J/(kg K) for $400°C \leq T \leq 1200°C$ (Eq 3.8)

The variation of thermal conductivity with temperature is proposed in Eurocode 2 through equations that describe upper and lower limits. In the present model, an average of the upper and lower bounds is used, described by the following equation.

$\lambda_c = 1.68–0.1906(T/100)+0.0082(T/100)^2$ W/(m K) for $20°C \leq T \leq 1200°C$ (Eq 3.9)

The impact of the reinforcing steel on the heat transfer can be neglected in an analysis, since the relatively small cross-sectional area of steel is expected to have a negligible effect on the conductivity and thermal capacity of the RC section.

3.3.2 Material Models: Effect of Elevated Temperature on Mechanical Properties

This section presents the material models used to describe the mechanical properties of concrete and reinforcing steel. The mechanical properties are required for the structural analysis to determine the stress and strain distribution in the concrete structure. The mechanical properties in this section include compressive strength, tensile strength of concrete, thermal strain in concrete, creep and transient strain in concrete, yield strength of steel, modulus of elasticity of steel, ultimate strain of steel, and thermal strain in steel.

3.3.2.1 Compressive Strength of Concrete

The formulation for compressive strength of concrete at elevated temperatures was developed using experimental data from Anderberg and Thelandersson (1976). In their testing, concrete specimens were heated to a target temperature and then loaded to failure to record stress-strain curves for concrete at elevated temperatures. The values of peak compressive stress for each temperature tested are used in this study to derive a mathematical relationship for the dependence of compressive strength on temperature. For temperatures up to 400°C, there is not a significant drop in compressive strength. For temperatures above 400°C, a quadratic curve fit was applied to the data to determine the reduction in compressive strength. The ratio of the compressive strength at elevated temperature to the room-temperature compressive strength, i.e. the stress reduction factor, is given by the following equations.

$$\sigma_{uT} / \sigma_{u0} = 1 \qquad \text{for } 20°C \leq T \leq 400°C \qquad \text{(Eq 3.10)}$$

$$\sigma_{uT}/\sigma_{u0} = 3.649\text{x}10^{-6}\, T^2 - 6.259\text{x}10^{-3}\, T + 2.845 \qquad \text{for } 400°C < T \leq 770°C \qquad \text{(Eq 3.11)}$$

where σ_{uT} is the compressive strength at temperature T, and σ_{u0} is the compressive strength at 20°C.

The above relationship was used in the present study because experimental stress-strain curves for concrete that is unstressed during heating are available for validation analyses, whereas full stress-strain curves for concrete that is stressed during heating are not readily available. However, the concrete in a structure exposed to fire will likely be stressed during heating due to gravity loads. Concrete that is stressed during heating does not show the same drop in compressive strength at elevated temperatures as concrete that is unstressed. For this reason, a different stress reduction factor should be used in future analyses for structures in fire. An example of a model for the compressive strength of concrete that is stressed during heating is presented in Knaack et al. (2009), who gathered data from 14 experimental studies and performed multiple regression analysis to determine a relationship for the compressive strength at elevated temperatures. The compressive strength loss of concrete at elevated temperatures is proposed by Knaack et al. (2009) in the following equation.

$$\sigma_{uT} / \sigma_{u0} = \kappa_{fm0} + \kappa_{fm1} T + \kappa_{fm2} T^2 + \kappa_{fm3} T^3 \quad \text{(Eq 3.12)}$$

where T is in °F, σ_{uT} is the compressive strength at temperature T, σ_{u0} is the compressive strength at 68°F (20°C), and the κ regression coefficients for normal strength concrete are based on aggregate type (siliceous versus calcareous) and testing method (residual, stressed, or unstressed). The siliceous category includes sandstone and materials containing large amounts of quartz, and the calcareous category includes carbonate, limestone, and dolomite (Knaack et al. 2009). The most appropriate test type to use for structures subjected to fire is the "stressed" category, which is when a specimen is loaded to a given preload (typically 30-50% of compressive strength), heated to a specified temperature, and then loaded to failure. The regression coefficients are given in Table 3.1.

Table 3.1. Regression coefficients for compressive strength loss model (Knaack et al. 2009).

	NSC					
	Siliceous			Calcareous		
	Residual	Stressed	Unstressed	Residual	Stressed	Unstressed
κ_{fm0}	0.963	0.995	0.953	0.997	1.023	0.981
κ_{fm1}	6.45E-04	8.42E-05	7.89E-04	6.51E-05	-4.00E-04	3.11E-04
κ_{fm2}	-1.64E-06	-9.02E-08	-1.65E-06	-3.13E-07	1.11E-06	-5.41E-07
κ_{fm3}	5.46E-10	-1.89E-10	5.28E-10	-6.75E-11	-7.00E-10	1.76E-11
Temperature range (°C)	[20,800]	[20,817]	[20,871]	[20,800]	[20,818]	[20,871]
Compressive strength range (psi)	[3900,5500]	[3900,5500]	[3900,5500]	[3542,6000]	[3900,5600]	[1149,6000]
R^2	0.90	0.92	0.93	0.86	0.61	0.69

3.3.2.2 Tensile Strength of Concrete

The reduction in tensile strength of concrete at elevated temperatures is given by the following equations, provided in EC 2 (CEN 2004).

$$f_{tT}(T) = k_t(T)\, f_{t0} \qquad \text{(Eq 3.13)}$$

$k_t(T) = 1.0$ for $20°C \leq T \leq 100°C$
$k_t(T) = 1.0 - 1.0\,(T-100)/500$ for $100°C \leq T \leq 600°C$

where f_{t0} is the tensile strength at room temperature. For the present study, a simplification was made by assuming that the reduction in tensile strength was equal to the reduction in compressive strength at elevated temperatures. This allows for the use of one stress reduction factor, given in (Eq 3.10) and (Eq 3.11), for both compressive and tensile stresses.

3.3.2.3 Thermal Strain in Concrete

The thermal strain of concrete depends on temperature and on the aggregate type, i.e. on whether siliceous or calcareous aggregate is used. Expressions for concrete with calcareous aggregate are used in the present study. According to EC2, the thermal strain for calcareous aggregate concrete is given by the following expressions.

$$\varepsilon_{th}(T) = -1.2x10^{-4} + 6x10^{-6}\,T + 1.4x10^{-11}\,T^3 \quad \text{for } 20°C \le T \le 805°C \quad \text{(Eq 3.14)}$$

$$\varepsilon_{th}(T) = 12x10^{-3} \quad \text{for } 805°C \le T \le 1200°C \quad \text{(Eq 3.15)}$$

The following expressions are provided in EC2 to allow the estimation of the thermal strain for concrete with siliceous aggregate.

$$\varepsilon_{th}(T) = -1.8x10^{-4} + 9x10^{-6}\,T + 2.3x10^{-11}\,T^3 \quad \text{for } 20°C \le T \le 700°C \quad \text{(Eq 3.16)}$$

$$\varepsilon_{th}(T) = 14x10^{-3} \quad \text{for } 805°C \le T \le 700°C \quad \text{(Eq 3.17)}$$

3.3.2.4 Creep Strain and Transient Strain in Concrete

Creep strain occurs when a specimen is under a constant load for a long period of time. Creep strain is more pronounced at higher temperatures (Knaack et al. 2009). Transient strain is a negative (compressive) strain caused by a chemical reaction in the concrete that occurs when the concrete undergoes its first heating cycle under compressive stress. The transient strain is irreversible and can comprise a significant portion of the total strain (Anderberg and Thelandersson 1976). These strain components must be added to the mechanical and thermal strains to capture better the impact of elevated temperatures on the stress-strain relation of concrete.

The creep strain in concrete can be modeled by the equation proposed by Anderberg and Thelandersson (1976), which was given in Li and Purkiss (2005) as:

$$\varepsilon_{cr}(\sigma, T, t) = -0.00053\,(\sigma/\,\sigma_{uT})\,(t/180)^{0.5}\,e^{0.00304(T-20)} \quad \text{(Eq 3.18)}$$

where T is the temperature in °C, t is the time in minutes, and σ_{uT} is the peak compressive stress at temperature T (which can be determined using the above model for compressive stress as a function of temperature).

Anderberg and Thelandersson (1976) also proposed an equation for the transient strain in concrete, which was given in Li and Purkiss (2005) as:

$$\varepsilon_{tr} = -k_{tr} (\sigma / \sigma_{u0}) \varepsilon_{th} \quad \text{for } T \leq 550°C \quad \text{(Eq 3.19)}$$

$$\partial\varepsilon_{tr}/\partial T = -0.0001 (\sigma / \sigma_{u0}) \quad \text{for } T \geq 550°C \quad \text{(Eq 3.20)}$$

where k_{tr} is a constant with value between 1.8 and 2.35 (Anderberg and Thelandersson 1976), σ_{u0} is peak compressive stress at room temperature, and ε_{th} is the thermal strain in the concrete.

3.3.2.5 Yield Strength and Modulus of Elasticity of Reinforcing Steel

The modification in the steel stress-strain law is based on the expressions by EC2, which establish a reduction in the modulus of elasticity and yield strength of the material at elevated temperatures. Reduction coefficients are tabulated for various temperatures, as shown in Table 3.2. These coefficients can be multiplied by the room-temperature yield strength and modulus of elasticity to determine the yield strength and modulus of elasticity at elevated temperature T.

Table 3.2. Reduction in elastic modulus and yield strength of reinforcing bars at elevated temperatures (CEN 2004).

Steel	f_{yT}/f_{y0}		E_T/E_0	
Temperature (°C)	hot rolled	cold worked	hot rolled	cold worked
20	1.00	1.00	1.00	1.00
100	1.00	1.00	1.00	1.00
200	1.00	1.00	0.90	0.87
300	1.00	1.00	0.80	0.72
400	1.00	0.94	0.70	0.56
500	0.78	0.67	0.60	0.40
600	0.47	0.40	0.31	0.24
700	0.23	0.12	0.13	0.08
800	0.11	0.11	0.09	0.06
900	0.06	0.08	0.07	0.05
1000	0.04	0.05	0.04	0.03
1100	0.02	0.03	0.02	0.02
1200	0.00	0.00	0.00	0.00

3.3.2.6 Ultimate Strain in Reinforcing Steel

The ultimate strain of reinforcing steel at elevated temperatures is given by EC2 as ε_{uT} = 0.1 for cold worked reinforcement and ε_{uT} = 0.2 for hot rolled reinforcement. The stress-strain relationship for steel in EC2 does not account for strain hardening in the material.

3.3.2.7 Thermal Strain in Reinforcing Steel

EC2 provides the following expressions for the thermal strain of reinforcing steel.

$\varepsilon_{s,th}(T) = -2.416x10^{-4} + 1.2x10^{-5} T + 0.4x10^{-8} T^2$ for $20°C \leq T \leq 750°C$ (Eq 3.21)

$\varepsilon_{s,th}(T) = 11x10^{-3}$ for $750°C \leq T \leq 860°C$ (Eq 3.22)

$\varepsilon_{s,th}(T) = -6.2x10^{-3} + 2x10^{-5} T$ for $860°C \leq T \leq 1200°C$ (Eq 3.23)

3.3.2.8 Creep Strain in Reinforcing Steel

The creep strain in reinforcing steel is not explicitly taken into account in the nonlinear truss model because it is implicitly modeled in the Eurocode stress-strain formulation (Bamonte and Lo Monte 2015; Wang et al. 2013b) and because the creep strain does not have a significant effect for the typical duration and loading in a fire (Bamonte and Lo Monte 2015).

3.4 Description of Truss Analysis for Coupled Thermo-mechanical Models

There are two aspects of incorporating the above material models into the nonlinear truss model: using the thermal properties to perform a heat transfer analysis and using the mechanical properties to determine the stresses and strains in the structure. The heat transfer analysis is used to determine the temperature distribution in the concrete at each time step. The temperature of the concrete is then used to determine the mechanical properties of the material for use in the structural analysis. The two analyses are coupled, because the results of the thermal analysis

affect the mechanical analysis. A schematic of the global solution scheme is illustrated in Figure 3.6. The steps in the solution process are detailed in the following sections.

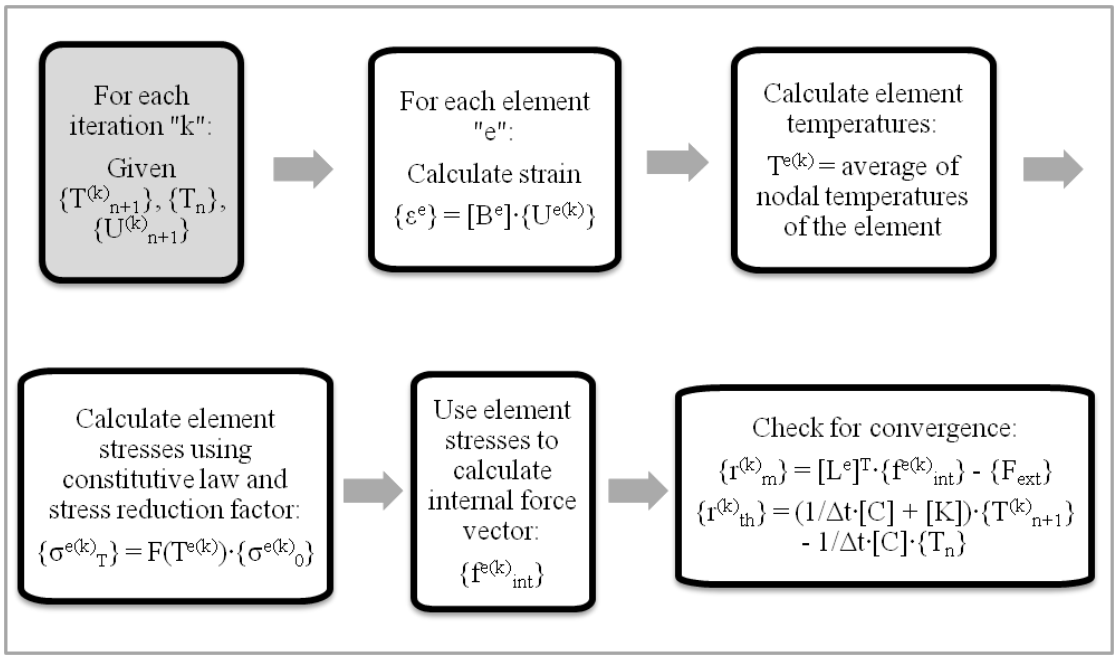

Figure 3.6. Schematic of global solution scheme.

3.4.1 Heat Transfer Analysis

The thermal properties of concrete, namely the thermal conductivity and the specific heat, affect how heat from a fire travels through the interior of the RC structure. The temperature of a fire can be described by various time-temperature curves given in design manuals and literature, as outlined in the literature review. The fire curve that is commonly used in experimental and analytical studies is the ASTM E119 curve (ASTM 2014). In general, the temperature distribution in a concrete member is a function of spatial coordinates and time. The temporal and spatial distribution of the temperature is described by the following partial differential equation and boundary/initial conditions.

$$\rho(T)\cdot c_p(T)\cdot \dot{T} + \vec{\nabla}\cdot([D]\{\nabla T\}) + s(x,y,z,t) = 0, \text{ where } [D] = \lambda_c(T)\cdot \begin{bmatrix} 1 & 0 \\ 0 & 1 \end{bmatrix} \quad \text{(Eq 3.24)}$$

$$T = \overline{T}(t) \text{ on } \Gamma_T$$

$$\vec{n} \cdot \vec{q} = \bar{q}(t) \text{ on } \Gamma_q$$

$$T(x,y,z,t=0) = T_0(x,y,z)$$

When the finite element semi-discretization is used for the problem, an initial-value problem for the nodal temperature values results, which is given by the following equation.

$$[C]\cdot\{\dot{T}\} + [K]\cdot\{T\} = \{f\} \quad \text{(Eq 3.25)}$$

where [C] is the global (structural) heat capacity matrix, [K] is the global conductance matrix, and {f} is the global nodal flux vector. The global matrices and vector are obtained from assembly of the corresponding element arrays. The element heat capacity and conductance arrays and the element nodal flux vector are given by the following equations.

$$[c^{(e)}] = \iiint_{\Omega^{(e)}} \left[N^{(e)}\right]^T \rho^{(e)}\, c_p{}^{(e)}\, [N^{(e)}]\, dV \quad \text{(Eq 3.26)}$$

$$[k^{(e)}] = \iiint_{\Omega^{(e)}} \left[B^{(e)}\right]^T [D^{(e)}]\, [B^{(e)}]\, dV \quad \text{(Eq 3.27)}$$

$$\{f^{(e)}\} = \iiint_{\Omega^{(e)}} \left[N^{(e)}\right]^T s\, dV + \iint_{\Gamma_q^{(e)}} \left[N^{(e)}\right]^T \bar{q}\, dS \quad \text{(Eq 3.28)}$$

The dependence of the density, specific heat, and conductivity on temperature can be introduced in the finite element model using the expressions described in Section 3.2.

In this study, a simplification is made by assuming that the heat capacity and conductivity remain constant throughout an analysis. The effect of fire in a compartment is incorporated in an

analysis by prescribing the temperature on the surfaces of the members in the compartment, as illustrated by the schematic in Figure 3.7. As a first step, the flux on the natural boundary and the heat source are assumed to be zero. If the nodal temperatures at some time step "n" are known, then the temperatures at the next time step, "n+1", can be obtained as follows. First, (Eq 3.25) is integrated with respect to time, between time steps "n" and "n+1".

$$\int_{t_n}^{t_{n+1}} [C] \cdot \{\dot{T}\} dt + \int_{t_n}^{t_{n+1}} [K] \cdot \{T\} dt = \{0\} \quad \text{(Eq 3.29)}$$

$$[C] \cdot \{T_{n+1}\} - [C] \cdot \{T_n\} + \int_{t_n}^{t_{n+1}} [K] \cdot \{T\} dt = \{0\} \quad \text{(Eq 3.30)}$$

Using the Backward Euler method (Hughes 2000), an approximation is introduced for the second integral in the above equation, where

$$\int_{t_n}^{t_{n+1}} [K] \cdot \{T\} dt \cong [K] \cdot \{T_{n+1}\} \cdot \Delta t, \quad \text{where} \quad \Delta t = t_{n+1} - t_n \quad \text{(Eq 3.31)}$$

Substituting (Eq 3.31) into (Eq 3.30) yields the following equation.

$$[C] \cdot \{T_{n+1}\} - [C] \cdot \{T_n\} + [K] \cdot \{T_{n+1}\} \cdot \Delta t = \{0\} \quad \text{(Eq 3.32)}$$

Dividing by Δt and solving for $\{T_{n+1}\}$ results in an equation for the nodal temperatures at time step n+1 as a function of the nodal temperatures at time step n.

$$\{T_{n+1}\} = (1/\Delta t \cdot [C] + [K])^{-1} \cdot (1/\Delta t \cdot [C] \cdot \{T_n\}) \quad \text{(Eq 3.33)}$$

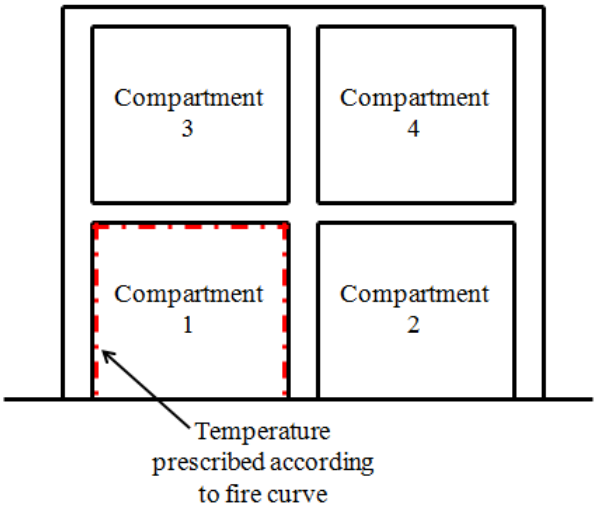

Figure 3.7. Prescribed temperatures for a fire in compartment 1.

For the present study, the fire temperature is assumed to be given by the ASTM E119 curve (shown in Figure 3.8). The ASTM standard provides a tabulated form of the time-temperature data, where the data is provided at 5-minute increments from 20 degrees C to 1010 degrees C and 10-minute increments from 1010 degrees C to 1260 degrees C. Kodur et al. (2008) proposed an equation for the temperature as a function of time that approximates the ASTM E119 fire curve, which is given by the following equation.

$$T = 20 + 750(1-\exp(-3.79553\sqrt{t})) + 170.41\sqrt{t} \quad \text{(Eq 3.34)}$$

where t is time in hours and T is the room temperature in degrees Celsius. This equation was used in the current research since the temperature had to be described in terms of a mathematical equation.

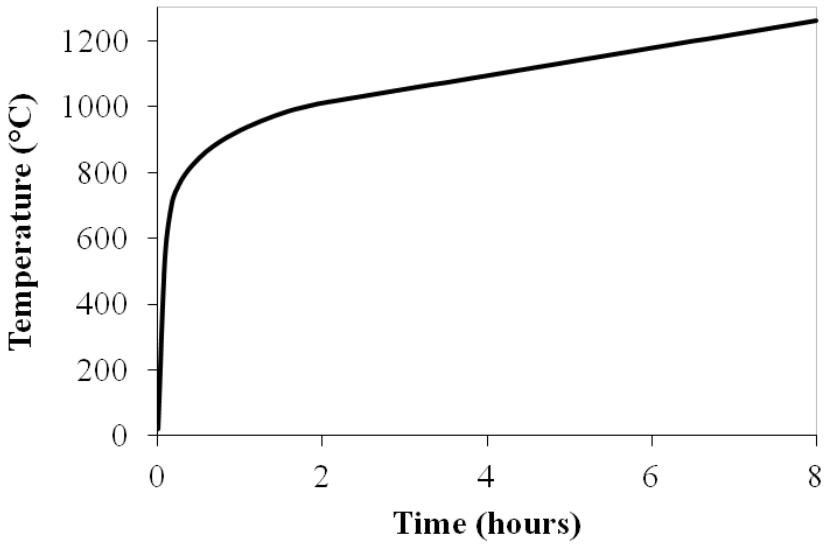

Figure 3.8. Temperature-time curve from ASTM E119 (ASTM 2014).

3.4.2 Mechanical (Stress) Analysis

The nonlinear finite element analysis of the RC truss structures was accomplished using the Newton-Raphson iterative procedure in FEAP. At each time step, trial values for the nodal displacements are assumed and used to calculate the strains in each element. The strains are used in the constitutive laws to obtain the stresses in each element, which are used to calculate the internal force vector. If the residual between the trial internal force vector and the external load vector is below a specified tolerance value, then the trial values of the displacements are stored. If the residual is larger than the specified tolerance, then a new set of trial values for the nodal displacements is calculated and the procedure is repeated. This iteration continues until the residual is below the specified tolerance. Figure 3.6 provides a schematic representation of this process.

The truss elements in the FEAP model are corotational, meaning that the axial direction of each element changes as the element deforms. A corotational formulation naturally captures

the effects of geometric nonlinearities on truss members. Because thermal expansion can cause large displacements in RC structures during fire, capturing the geometric nonlinearities is necessary to obtain accurate solutions.

For the mechanical analysis, the existing nonlinear truss model must be modified so that it accounts for the changes in the stress-strain laws of concrete and steel at elevated temperatures. The stress-strain laws are primarily changed in three ways: increase in strain, reduction in strength, and increase in deformability.

3.4.2.1 Modifications to Concrete Constitutive Relationship

The total concrete strain at elevated temperatures is composed of thermal strain, creep strain, transient strain, and mechanical strain. The existing constitutive relationships in the nonlinear truss model are functions of the mechanical strains in the concrete. At room temperature, there are no transient or thermal strains, and creep strain does not have any significant effect on the structural behavior, so the total strain is equal to the mechanical strain. However, at elevated temperatures, the total strain in the concrete is composed of mechanical strain, thermal strain, transient strain, and creep strain. In order to maintain compatibility with the existing stress-strain relationship in the nonlinear truss model, the mechanical strain must be separated from the other strain components. For each iteration of the Newton-Raphson method, the total strain in each element is calculated using the trial nodal displacements. The thermal strain in (Eq 3.14) and (Eq 3.15), transient strain in (Eq 3.19) and (Eq 3.20), and creep strain in (Eq 3.18) are calculated and then subtracted from the total strain to obtain the mechanical strain:

$$\varepsilon_m = \varepsilon_{total} - \varepsilon_{th} - \varepsilon_{tr} - \varepsilon_{cr} \quad \text{(Eq 3.35)}$$

Because the creep strain and the transient strain depend upon the current stress in the material, iterative procedures must be used to determine their values. These procedures are detailed in Section 3.4.2.1.1. The mechanical strain is then used in the constitutive relationships to determine the stress in each element.

The reduction in strength for concrete is accounted for by multiplying the stress, $\sigma_0(\varepsilon_m)$, by a reduction factor. At each time step in the finite element analysis, the stress in each element is determined using the calculated mechanical strain (Eq 3.35) and the existing stress-strain relationships (i.e. no thermal effects), and then it is multiplied by the reduction factor, which is a function of the current temperature of the material.

$$\sigma_T(\varepsilon_m, T) = F(T)\cdot\sigma_0(\varepsilon_m) \qquad \text{(Eq 3.36)}$$

where σ_T is the stress accounting for the effect of elevated temperature, σ_0 is the room-temperature stress obtained from the existing stress-strain relationship, and the strength reduction factor, F(T), is given by (Eq 3.12).

The increased deformability of concrete at elevated temperatures is implicitly accounted for by using the strength reduction factor and including the temperature-induced strains in the strain formulation.

A flowchart detailing the procedure for incorporating temperature effects into the concrete constitutive relationship is shown in Figure 3.9.

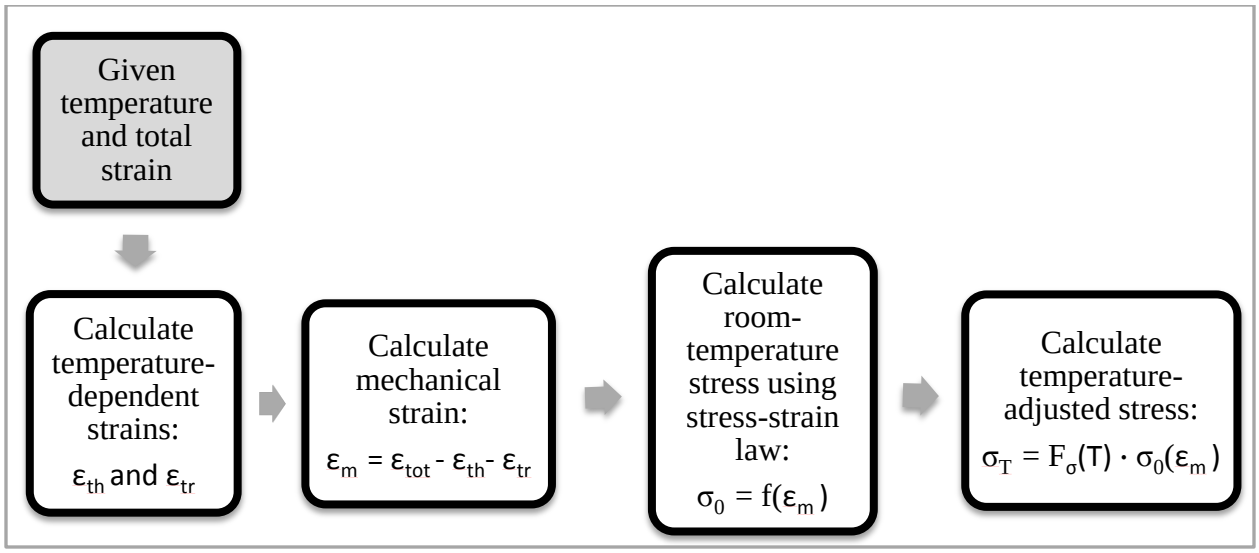

Figure 3.9. Procedure for incorporating temperature effects into concrete constitutive relationship.

3.4.2.1.1 Iterative Procedure for Determining Transient Strain

The equations proposed by Anderberg and Thelandersson (1976) for creep and transient strain both depend upon the current value of the stress in the element. However, calculating the stress in the element requires the mechanical strain, which is dependent upon the transient and creep strains (Eq 3.35). Because all of these values are interrelated, an iterative procedure using the rate form of transient strain must be used in order to converge on the correct values for each term at each time step. In the present analysis, the creep strain is neglected to simplify the procedure and because research suggests that it is a small portion of the total strain for typical fire scenarios (Li and Purkiss 2005).

The transient strain equation for T > 550°C is in terms of a derivative with respect to time. In order to obtain the rate form of transient strain, the integral of this equation must be determined first. Taking the integral of (Eq 3.20) yields the following equation.

$$\varepsilon_{tr} = -0.0001\,(\sigma/\,\sigma_{u0})\cdot T + C \qquad \text{(Eq 3.37)}$$

where C is a constant. This integral was taken assuming that σ remains constant with respect to temperature, which is a reasonable assumption since the Anderberg and Thelandersson (1976) experiments that the equation is based upon were performed under constant stress. The constant C can be solved for by equating (Eq 3.37) with (Eq 3.19) at temperature T = 550°C. This results in the following equation.

$$C = (-k_{tr}\cdot\varepsilon_{th,550} + 0.055)\cdot(\sigma/\,\sigma_{u0}) \qquad \text{(Eq 3.38)}$$

where $\varepsilon_{th,550}$ is the thermal strain at 550°C, which is evaluated as 0.0055 using (Eq 3.14). The resulting transient strain for temperatures above 550°C is then given by the following equation.

$$\varepsilon_{tr} = -0.0001\cdot(\sigma/\,\sigma_{u0})\cdot T + 0.0055\cdot(-k_{tr} + 10)\cdot(\sigma/\,\sigma_{u0}) \qquad \text{for } T > 550\ °C \qquad \text{(Eq 3.39)}$$

Taking the derivative of (Eq 3.19) and (Eq 3.39) with respect to time, the rate form of the transient strain is given by the following equations.

$$\dot{\varepsilon}_{tr} = -k_{tr}\,(\dot{\sigma}/\,\sigma_{u0})\,\varepsilon_{th} - k_{tr}\,(\sigma/\,\sigma_{u0})\,\dot{\varepsilon}_{c,th} \qquad \text{for } T \leq 550\ °C \qquad \text{(Eq 3.40)}$$

$$\dot{\varepsilon}_{tr} = -0.0001\,(\dot{\sigma}/\,\sigma_{u0})\cdot T - 0.0001\cdot(\sigma/\,\sigma_{u0})\cdot dT/dt + 0.0055\cdot(-k_{tr} + 10)\cdot(\dot{\sigma}/\,\sigma_{u0}) \qquad \text{for } T > 550\ °C \qquad \text{(Eq 3.41)}$$

To convert to the discrete form of the rate equation, the time derivative of a function is approximated as $\dot{f} \approx \Delta f/\Delta t$. Using the midpoint rule, the terms in the discrete form will be evaluated at step n+1/2 where $f_{n+1/2} = \frac{1}{2}(f_n + f_{n+1})$. The discrete form of the rate equation is given by the following equations.

$$\Delta \varepsilon_{tr} = -k_{tr} (\Delta\sigma/ \sigma_{u0}) \varepsilon_{th,n+1/2} - k_{tr} (\sigma_{n+1/2}/ \sigma_{u0}) \Delta\varepsilon_{th} \quad \text{for } T \leq 550\ ^\circ C \quad \text{(Eq 3.42)}$$

$$\Delta \varepsilon_{tr} = -0.0001 (\Delta\sigma/ \sigma_{u0})\cdot T_{n+1/2} - 0.0001\cdot(\sigma_{n+1/2}/ \sigma_{u0})\cdot\Delta T + 0.0055\cdot(-k_{tr} + 10)\cdot(\Delta\sigma/ \sigma_{u0}) \quad \text{for } T > 550\ ^\circ C \quad \text{(Eq 3.43)}$$

Plugging in $f_{n+1/2} = \frac{1}{2}(f_n + f_{n+1})$ and $\Delta f = f_{n+1} - f_n$ yields the following equations.

$$\varepsilon_{tr,n+1} - \varepsilon_{tr,n} = -k_{tr} (\sigma_{n+1} - \sigma_n)/\sigma_{u0} \cdot (\varepsilon_{th,n+1} + \varepsilon_{th,n})/2 - k_{tr} (\sigma_{n+1} + \sigma_n)/ (2\sigma_{u0}) \cdot (\varepsilon_{th,n+1} - \varepsilon_{th,n}) \quad \text{for } T \leq 550\ ^\circ C \quad \text{(Eq 3.44)}$$

$$\varepsilon_{tr,n+1} - \varepsilon_{tr,n} = -0.0001 (\sigma_{n+1} - \sigma_n)/\sigma_{u0}\cdot(T_{n+1}+ T_n)/2 - 0.0001\cdot(\sigma_{n+1}+ \sigma_n)/ (2\sigma_{u0})\cdot(T_{n+1}-T_n) + 0.0055\cdot(-k_{tr} + 10)\cdot(\sigma_{n+1}- \sigma_n)/\sigma_{u0} \quad \text{for } T > 550\ ^\circ C \quad \text{(Eq 3.45)}$$

Solving for σ_{n+1} yields the following equations.

$$\sigma_{n+1} = 1/(F_1 + F_2) \cdot [\varepsilon_{tr,n+1} - \varepsilon_{tr,n} + \sigma_n (F_1 - F_2)] \quad \text{for } T \leq 550\ ^\circ C \quad \text{(Eq 3.46)}$$

where $F_1 = -k_{tr}/ \sigma_{u0} \cdot (\varepsilon_{th,n+1} + \varepsilon_{th,n})/2$

$F_2 = - k_{tr}/\sigma_{u0} \cdot (\varepsilon_{th,n+1} - \varepsilon_{th,n})/2$

$$\sigma_{n+1} = 1/(F_3+F_4+F_5)\cdot[\varepsilon_{tr,n+1} - \varepsilon_{tr,n} + \sigma_n(F_3 - F_4+F_5)] \quad \text{for } T > 550\ ^\circ C \quad \text{(Eq 3.47)}$$

where $F_3 = -0.0001/\sigma_{u0}\cdot(T_{n+1}+ T_n)/2$

$F_4 = - 0.0001/\sigma_{u0}\cdot(T_{n+1}-T_n)/2$

$F_5 = 0.0055\cdot(-k_{tr} + 10)/\sigma_{u0}$

All terms evaluated at time step "n" are known values, ε_{th} evaluated at time step "n+1" is known because it depends on temperature alone, and k_{tr} and σ_{u0} are known constants. The only unknowns are σ_{n+1} and $\varepsilon_{tr,n+1}$. At this point, iteration must be used since there are two unknowns and one equation. The iterative procedure is accomplished in the following steps:

1. Select a trial value of the transient strain at time t_{n+1}, and plug this into (Eq 3.46) if $T \leq 550°C$ or (Eq 3.47) if $T > 550°C$ to obtain the stress.
2. Using the trial value of transient strain, calculate the mechanical strain at time t_{n+1} using (Eq 3.35). Calculate the stress at time t_{n+1} based on the mechanical strain, the constitutive relationships, and the stress reduction factor.
3. Calculate the difference between the stress from step 1 and the stress from step 2 (i.e. the residual). If the residual is greater than the specified tolerance value, select a new trial value of transient strain and repeat steps 1-3 until the residual is less than the specified tolerance.

The residual for step 3 is given by the following equations.

$$r = 1/(F_1 + F_2) \cdot [\varepsilon_{tr,n+1} - \varepsilon_{tr,n} + \sigma_n (F_1 - F_2)] - \sigma_T(\varepsilon_{m,n+1}) \qquad \text{for } T \leq 550\ °C \qquad \text{(Eq 3.48)}$$

$$r = 1/(F_3+F_4+F_5)\cdot[\ \varepsilon_{tr,n+1}-\varepsilon_{tr,n}+\sigma_n(F_3-F_4+F_5)] - \sigma_T(\varepsilon_{m,n+1}) \qquad \text{for } T > 550\ °C \qquad \text{(Eq 3.49)}$$

where $\sigma_T(\varepsilon_{m,n+1})$ is the temperature-adjusted stress from the constitutive relationship in the nonlinear truss model, given by (Eq 3.36). If the residual is below a specified tolerance, then the procedure stops and $\varepsilon_{tr,n+1}$ and σ_{n+1} have been determined. If the residual is greater than the tolerance, then a new trial value of $\varepsilon_{tr,n+1}$ is chosen and the process is repeated. The new trial value of $\varepsilon_{tr,n+1}$ is chosen based on the Newton-Raphson iterative method, so that the new trial value is given by the following equation.

$$\varepsilon_{tr,n+1}^{k+1} = \varepsilon_{tr,n+1}^{k} - r^k/J^k \qquad \text{(Eq 3.50)}$$

$J^k = \partial r^k/\partial \varepsilon^k_{tr,n+1} = 1/(F_1 + F_2)$ for $T \leq 550$ °C

$J^k = \partial r^k/\partial \varepsilon^k_{tr,n+1} = 1/(F_3+F_4+F_5)$ for $T > 550$ °C

In the code used for the present research, the iterative form of the transient strain equations was not used in order to speed up computation time. Instead, the values of σ_{n+1} and σ_n in (Eq 3.44) and (Eq 3.45) were replaced with σ_n and σ_{n-1}, respectively. This results in an explicit form of the transient strain equation that depends on stress values at previous steps. The transient strain values "lag" behind by one time step, but this is a reasonable approximation for cases where the stress is not changing rapidly. In future work, the iterative procedure for determining transient strain is available for use and can be easily included in an analysis.

3.4.2.2 Modifications to Reinforcing Steel Constitutive Relationship

The increase in the strain in the reinforcing steel at elevated temperatures is due to the addition of thermal strain to the mechanical strain. In the present analysis, creep strain in the steel has been neglected for simplicity and because it does not have significant effect on the structural behavior during a typical fire scenario (Bamonte and Lo Monte 2015).

For steel elements, the changes in strength and modulus of elasticity will be described by the relationships given in Eurocode 2 (CEN 2004). The Eurocode relationships are proposed through tabulated data in Table 3.2. The finite element analysis requires that the reduction factors be given as an equation rather than tabulated data, so curve fitting was used to determine equations that adequately describe the relationships between temperature and the strength reduction factors for steel. A plot of the Eurocode values and the best-fit lines is shown in Figure

3.10. For the strength reduction factor, the best fit was obtained by defining a piecewise function, which is given by the following equations.

$$F_y(T) = f_{yT}/f_{y0} = 1 \qquad \text{for } T \leq 400\ ^\circ\text{C} \qquad \text{(Eq 3.51)}$$

$$F_y(T) = f_{yT}/f_{y0} \approx -1313\text{x}10^{-9}\ T^3 + 5.575\text{x}10^{-6}\ T^2 - 7.462\text{x}10^{-3}\ T + 3.213 \qquad \text{for } 400 < T \leq 1200\ ^\circ\text{C} \qquad \text{(Eq 3.52)}$$

where f_{yT} is the compressive strength at temperature T, and f_{y0} is the compressive strength at room temperature (20°C). For the elastic modulus reduction factor, the best fit was obtained using a fourth-order polynomial that is valid for temperatures between 20°C and 1200 °C, which is given by the following equation.

$$F_E(T) = E_T/E_0 \approx -2.295\text{x}10^{-12}\ T^4 + 7.372\text{x}10^{-9}\ T^3 - 7.075\text{x}10^{-6}\ T^2 + 1.05\text{x}10^{-3}\ T + 0.9631 \qquad \text{(Eq 3.53)}$$

where E_T is the elastic modulus at temperature T, and E_0 is the elastic modulus at room temperature (20°C). The reduction factor for the elastic modulus will not be used in the same way as the reduction factor for the strength, but rather it will be used indirectly to equate the Eurocode model with the existing constitutive relationship.

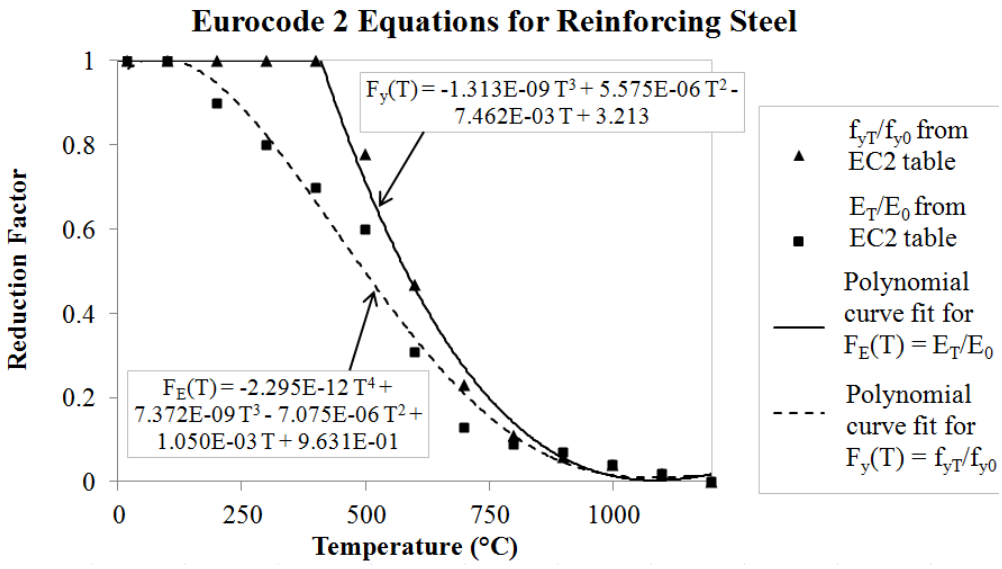

Figure 3.10. Approximate equations for the reduction factors in Eurocode 2.

Two different approaches can be taken to incorporate the thermal effects into the constitutive relationship for the reinforcing steel. The first is to separate the mechanical strain from the thermal strain and use the mechanical strain in the existing constitutive relationship with the strength reduction factor. This method implicitly reduces the modulus of elasticity of the steel at elevated temperatures. This method results in the following equations for strain and stress at elevated temperatures.

$$\varepsilon_m = \varepsilon_{total} - \varepsilon_{s,th} \qquad \text{(Eq 3.54)}$$

$$\sigma_T = F_y(T) \cdot \sigma(\varepsilon_m) \qquad \text{(Eq 3.55)}$$

where $\varepsilon_{s,th}$ is defined in (Eq 3.21) through (Eq 3.23), and $\sigma(\varepsilon_m)$ is the existing stress-strain law in the nonlinear truss model.

The second approach for changing the steel constitutive law is to prescribe equivalence of the stress from the Eurocode equations and the reduced stress from the existing constitutive law

at each mechanical strain value up to yield. If the stress from Eurocode 2 is defined as $\sigma_{EC} = E_T \varepsilon_{total} = F_E(T) \cdot E_0 \cdot \varepsilon_{total}$, and the stress from the existing stress-strain law is defined as $\sigma_{ex} = F_y(T) \cdot E_0 \cdot \varepsilon_m$, then equivalence is given by the following equation.

$$F_E(T) \cdot E_0 \cdot \varepsilon_{total} = F_y(T) \cdot E_0 \cdot (\varepsilon_{total} - \varepsilon_{s,th}) \quad \text{(Eq 3.56)}$$

If (Eq 3.56) is solved for $\varepsilon_{s,th}$, then the mechanical strain can be rewritten using the following equation.

$$\varepsilon_m = \varepsilon_{total} - \varepsilon_{s,th} = \varepsilon_{total} [\ F_E(T) / F_y(T)\ ] \quad \text{(Eq 3.57)}$$

This form of the mechanical strain can be used in the existing constitutive relationship with the stress reduction factor to determine the stress in the element, which results in a stress given by the following equation.

$$\sigma_T = F_y(T) \cdot \sigma(\varepsilon_m) \quad \text{(Eq 3.58)}$$

where $\sigma(\varepsilon_m)$ is the existing stress-strain law in the nonlinear truss model and ε_m is given by (Eq 3.57). This equation is based on the linear-elastic portion of the stress-strain relation in Eurocode 2, so it is valid for each point on the elastic portion of the proposed stress-strain curve. For plastic sections of the proposed stress-strain curve, the thermal strain will remain constant, and any change in the total strain will result in an equal change in the mechanical strain. This second approach was chosen for the present study because it allows for explicit use of the reduction functions for both strength and elastic modulus.

4 Validation Analyses

The implementation of the enhanced truss modeling approach in FEAP is validated through a series of analyses. The nonlinear truss method has been previously validated for earthquake response of RC walls (Panagiotou et al. 2012) and columns (Moharrami et al. 2014), but its adequacy for fire response modeling has not before been analyzed. The analyses presented here are based on material-level behavior of concrete and steel at elevated temperatures. Ensuring that the methods for incorporating temperature effects into the nonlinear truss elements can accurately capture temperature effects is critical for properly modeling structural systems.

4.1 Validation of Stress-strain Behavior at Elevated Temperatures

The stress-strain behavior of concrete at elevated temperatures using the enhanced nonlinear truss method in FEAP is compared with experimental data from Anderberg and Thelandersson (1976) in Figure 4.1. In the experimental tests, the specimens were heated to a target temperature and then loaded to failure. For both the analysis results and test data, the thermal strain that develops during heating has been subtracted out, so that the stress-strain plot starts at a strain of zero upon initial loading. The available data for the Anderberg and Thelandersson tests were for concrete specimens that were unstressed during heating, so (Eq 3.10) and (Eq 3.11) are used for the stress reduction factor to match the analysis with the testing conditions.

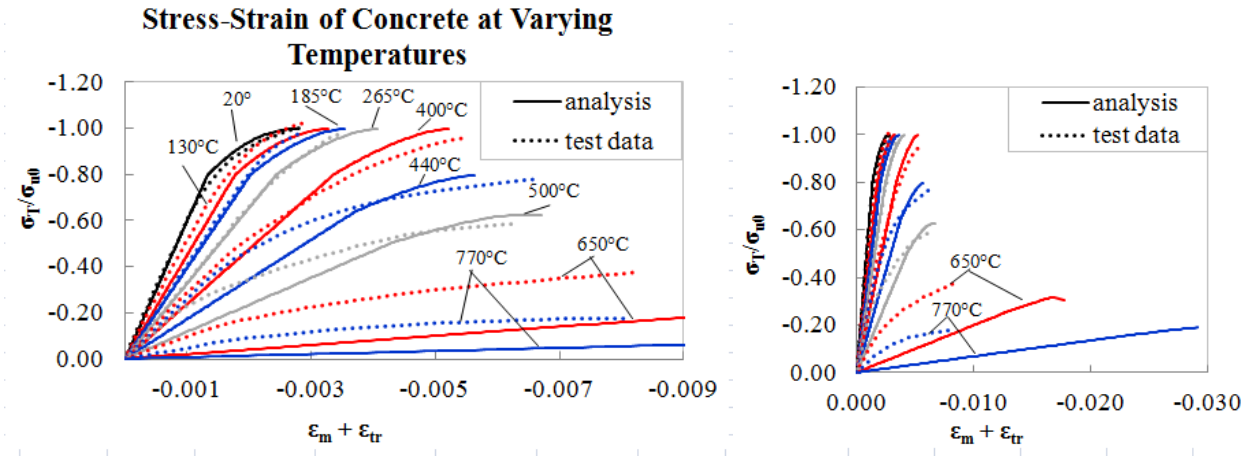

(a) (b)

Figure 4.1. (a) comparison of stress-strain behavior of concrete at elevated temperatures using nonlinear truss method with experimental data from Anderberg and Thelandersson (1976). (b) stress-strain of concrete at high temperature and large strains.

The analysis can satisfactorily reproduce the stress-strain behavior of concrete for temperature values between 20°C and 500°C. The FEAP model captures the reduction in the slope of the stress-strain diagram and compressive strength as temperature increases. It also captures the increased strain at peak stress due to the transient strains in the concrete. The best fit of the FEAP results with the test data was obtained with a transient strain coefficient, k_{tr}, of 0.8. This is lower than the values of 1.8-2.35 obtained by Anderberg and Thelandersson (1976), but their coefficients were calibrated using data from tests where the concrete was stressed during heating, which does not necessarily directly correlate to stress-strain behavior of concrete specimens unstressed during heating. The results illustrate that the enhanced nonlinear truss method is capable of capturing thermal effects on stress-strain behavior using an existing room-temperature constitutive relationship.

For the 650°C and 770°C cases, the strain is over predicted in the FEAP model. Figure 4.1(b) shows the 650°C and 770°C cases at larger strain values. The FEAP model is reaching the

appropriate peak stress value, but at a larger strain than the test data. This is due to the fact that the transient strain formulation changes at T = 550°C. The formulation for temperatures greater than 550°C appears to over predict significantly the transient strain when compared to the test data. Anderberg and Thelandersson reported that the transient strain formulation was not as accurate at temperatures greater than 550°C, and the transient strain is more difficult to predict due to the fact that the scatter between tests is larger at high temperatures (Anderberg and Thelandersson 1976). Because the strains were not being predicted appropriately, the transient strain formulation was updated so that (Eq 3.19) was used for the entire temperature regime, not just for temperatures less than 550°C. The results using this updated formulation are illustrated in Figure 4.2, and show a much better agreement with the experimental data. Further research into an appropriate formulation for transient strain for temperatures above 550°C is needed, but using this updated formulation provides a reasonable approximation at present.

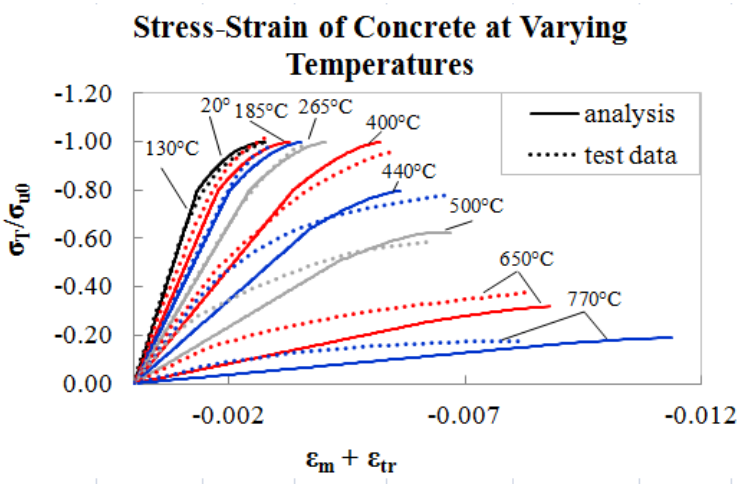

Figure 4.2. Comparison of stress-strain behavior of concrete at elevated temperatures using updated transient strain formulation with experimental data from Anderberg and Thelandersson (1976).

The stress-strain behavior of the reinforcing steel using the FEAP model is compared with test data for a Grade 50B (S275 equivalent in Eurocode) steel from Kirby and Preston (1988) in Figure 4.3. The FEAP model accurately captures the yield stress at elevated temperatures using the stress reduction factor and captures the reduction in Young's Modulus through the relationship in (Eq 3.58). Steel at elevated temperatures does not exhibit the same yield plateau that it exhibits at room temperature, but instead there is a gradual change in slope. This aspect is not captured by the FEAP results for monotonic loading because it is based on the existing stress-strain law used for the earthquake analysis, which includes a yield plateau. However, it is important to note that the stress-strain law used in the FEAP analysis includes nonlinear strain hardening regions. In the case of a post-earthquake fire, the reinforcing steel will likely have already entered the strain hardening region due to cyclic earthquake loads. At this point, the stress-strain curve will not exhibit a yield plateau, but will exhibit nonlinearity similar to the test results shown in Figure 4.2 for steel at elevated temperatures.

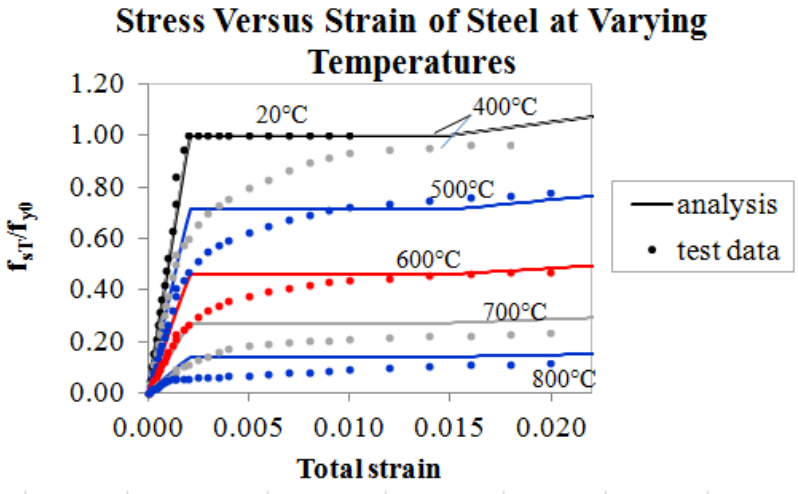

Figure 4.3. Comparison of stress-strain behavior of reinforcing steel at elevated temperatures using nonlinear truss method with experimental data from Kirby and Preston (1988).

4.2 Validation for heating concrete under constant stress

Transient strain in concrete can be best illustrated by comparing the strain in concrete during heating for specimens at different stress levels. Anderberg and Thelandersson (1976) conducted a test series where concrete specimens were pre-loaded with a percentage of compressive strength (ranging from 0% to 90%), and then the strain in the concrete was measured as the temperature was raised from 20°C to 800°C at a rate of 5°C/min. In Figure 4.4, this test data is compared with results from the FEAP model for a single concrete truss element heated to 800°C using a transient strain coefficient, k_{tr}, of 0.8. The mechanical strain due to the preload has been removed from the strain data so that all strain histories start at zero. The test data includes thermal, transient, and creep strains, whereas the FEAP model includes only thermal and transient strains. The 0% preload case represents the free thermal expansion (i.e. thermal strain) of concrete. As shown in the graph, the thermal strain in the FEAP model under predicts the thermal strain in the test data. This is due to the fact that the relationship for thermal strain in the FEAP model is based on calcareous aggregate concrete, and the Anderberg and Thelandersson (1976) tests were for a siliceous aggregate concrete. As a reference, the dash-dot line on the graph is the Eurocode equation for thermal strain of siliceous aggregate concretes, which matches more closely with the results obtained by Anderberg and Thelandersson (1976). The difference in materials partially accounts for the differences between the FEAP results and the test data since the thermal strain is one component of total strain, and because the transient strain formulation is a function of thermal strain. The creep strain has been neglected in the FEAP model, which is also responsible for a small difference between the test data and the FEAP results. Despite these differences, the FEAP model was able to predict the critical temperature for the 45% and 67.5% cases. The critical temperature is defined as the temperature

at which the concrete can no longer sustain the applied preload. The compressive strain in these two cases is under predicted compared with the experimental results. For the 22.5% and 35% load cases, the results match reasonably well until 550°C. As discussed above, this is the temperature at which the transient strain formulation changes. From Figure 4.4, it is clear that the strain is over predicted for these cases at temperatures above 550°C. This is likely due to the over prediction of transient strain, which is similar to what was seen in the stress-strain curve comparisons of Section 4.1.

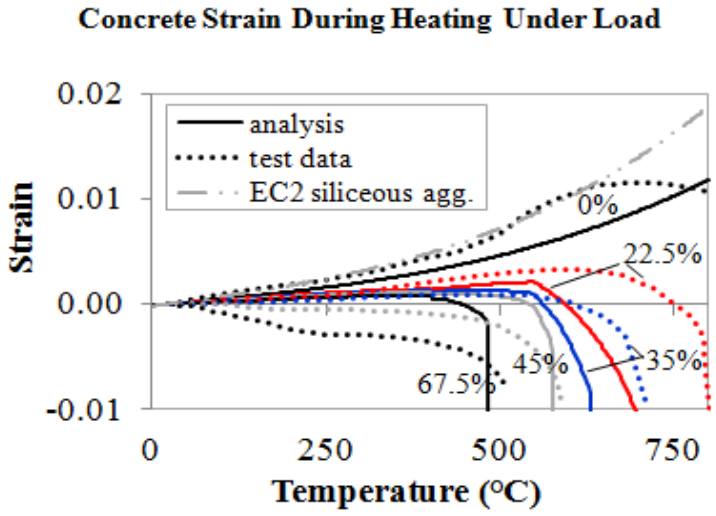

Figure 4.4. Comparison of concrete strain during heating under load using nonlinear truss method with experimental data from Anderberg and Thelandersson (1976). Heating rate for experimental test was 5°C/min.

The enhanced nonlinear truss model is capable of capturing the effect of preload on the strain in concrete during heating, but further refinement is needed in future research. Due to transient strain, the amount of preload can have a significant effect on the total strain in a concrete specimen. Because RC structures in fires have a preload due to dead and live loads, the effects of transient strain must be incorporated in any modeling or analysis of fire effects. The transient strain can be difficult to predict, particularly at high temperatures, but the enhanced

nonlinear truss method has the capabilities to incorporate transient strain formulations into existing stress-strain laws.

5 Verification of Modeling Approach for System-Level Analyses

After the implementation of the material models and the validation at the material level, it was deemed necessary to verify the capability of the modeling approach to allow system-level simulations. Specifically, the modeling approach is used to analyze a prototype reinforced concrete structure for two cases: earthquake loading and fire occurrence. The structure used in the analyses is taken from a seismic design example in the NEHRP Recommended Seismic Provisions document (FEMA 2012). This building has been designed according to the seismic requirements for a structure located in Berkeley, CA, which is an area characterized by high seismic activity. The structure is a 12-story reinforced concrete office building, with a girder span length of 40 ft. An elevation drawing of the structure is shown in Figure 5.1. This building is chosen because the member details are readily available and the structure has been designed for high seismicity. For simplicity, and given that this is merely a verification analysis, the analytical model does not include the basement level; the structure is assumed to be fixed at the ground level. Additionally, the analytical model uses a story height of 13 ft for all floors rather than using a different story height for the first floor. The gravity loads are introduced as nodal loads on the beams, and the values of the nodal loads are those corresponding to uniform distributed gravity forces due to dead loads and live loads.

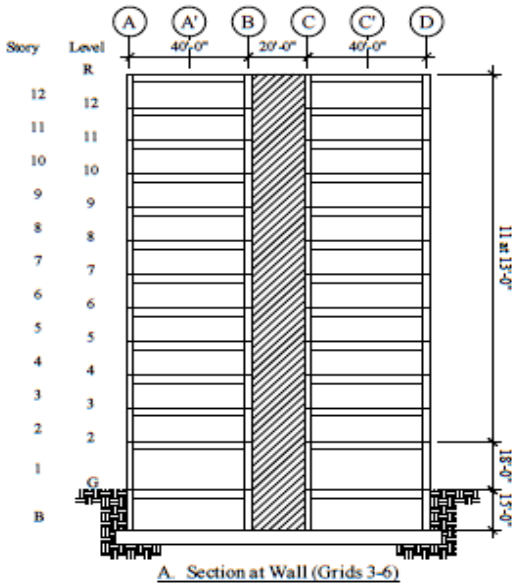

Figure 5.1. Elevation drawing of building from NEHRP Recommended Seismic Provisions (FEMA 2012).
FEMA. (2012). *FEMA P-751: 2009 NEHRP Recommended Seismic Provisions: Design Examples*. Used under fair use, 2015.

5.1 Analysis for Earthquake Loading

For the earthquake analysis, the structure is subjected to the Sylmar – Olive View (360) ground motion record from the 1994 Northridge, CA earthquake, shown in Figure 5.2. The Northridge earthquake had a moment magnitude of 6.7 and caused extensive structural damage in affected buildings. The peak horizontal roof displacement predicted in the FEAP model is 14.6 in., which corresponds to an average drift ratio of 0.77%. The time history of the average drift ratio is presented in Figure 5.3. This analysis verified that the proposed model can effectively analyze a structure subjected to earthquake loading through the use of truss elements representing the concrete and reinforcing steel.

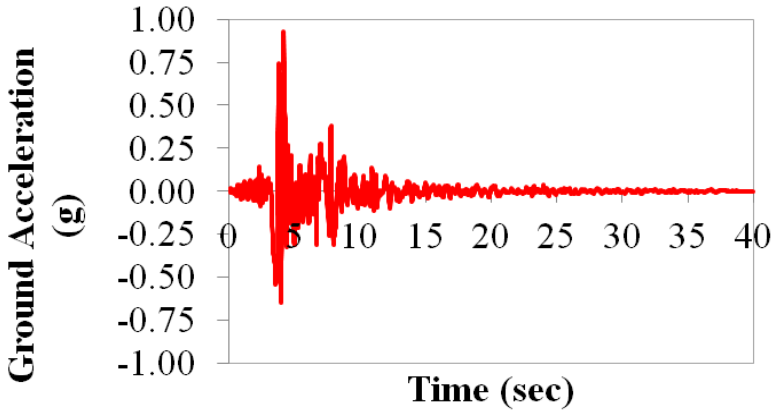

Figure 5.2. Sylmar – Olive View ground acceleration record from 1994 Northridge, CA earthquake.

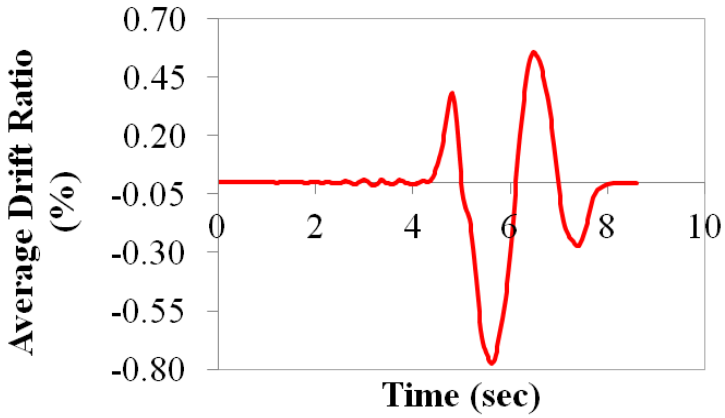

Figure 5.3. Average drift ratio as a function of time for FEAP analysis.

5.2 Fire Analysis

The second verification analysis corresponds to the occurrence of a fire at the left bay of the bottom story. The temperature at the nodes corresponding to the surface of the members of the specific bay of the structure are prescribed to evolve according to the ASTM E119 fire curve (ASTM 2014). The temperature contours for three time steps throughout the analysis are illustrated in Figure 5.4. The model is able to capture the temporal and spatial distribution of temperatures throughout the structure due to the spread of the fire. It is worth mentioning that the

temperatures of the members in the vicinity of the fire occurrence may be overestimated in this analysis. The reason for this potential overestimation is that the air in the compartments is not being modeled. In a realistic fire, an amount of heat will be emitted to the air surrounding the structure through convection. In the analytical model, the heat conduction problem is simplified and only includes diffusion within members. Effectively, this means that the boundaries of the beams and columns are insulated, and heat is "trapped" within the structure.

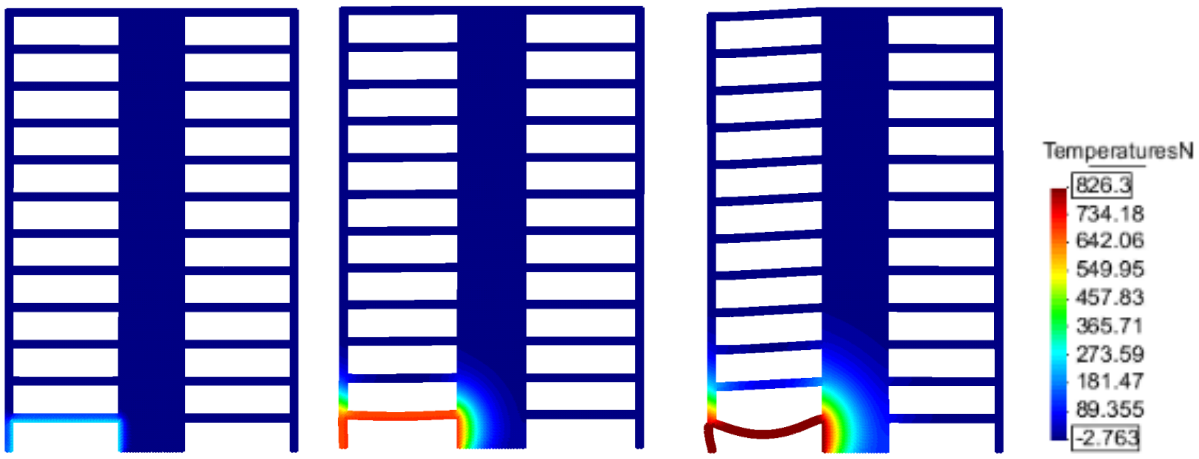

Figure 5.4. Temperature contours calculated by FEAP model at approximately 2 minutes, 10 minutes, and 25 minutes after the start of the fire exposure.

In terms of the mechanical behavior, the analytical model gives a global structural behavior that is qualitatively similar to the one observed in the Cardington fire tests. As the temperature in the floor beam increases, thermal expansion of the beam causes horizontal outward forces on the columns. This results in compression in the beam as the column resists the outward motion. Similarly, in the Cardington fire tests, the slabs exhibited compression membrane behavior due to the restraint from the surrounding room-temperature concrete (Chana and Price 2003). Towards the end of the analysis, the floor beam that is exposed to the fire

exhibits tensile membrane behavior due to the very large displacements (maximum vertical deflection of 68 in.), as illustrated in Figure 5.5. Specifically, the distributed gravity load on the beam is carried through tension in the steel truss elements, resulting in an ability to carry load despite severe deflection. The large displacements illustrate that using corotational elements in the FEAP model is appropriate and necessary for accurate prediction of mechanical behavior. Membrane behavior (tension or compression) is able to develop due to the restraint provided by supporting elements, and this type of interaction may not be accurately captured in component-level testing or modeling. These restraint forces can also cause spalling in concrete at elevated temperatures due to the increased compressive stresses (Bažant and Kaplan 1996). The thermal expansion and resulting compressive stresses are captured in the proposed model, so the loss of capacity due to restraint-induced spalling is accounted for. However, the spalling that is caused by water vapor pressure (the second spalling mechanism proposed by Bažant and Kaplan 1996) is not currently accounted for in the proposed model.

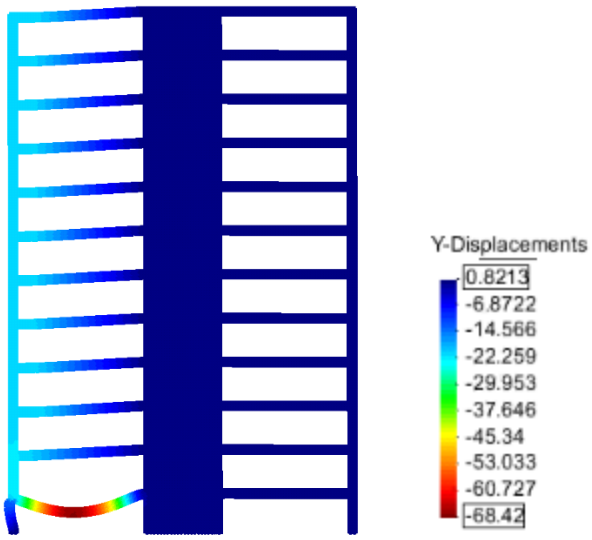

Figure 5.5. Y-displacement contours predicted by FEAP model prior to structural instability.

The outward deflection of the exterior column due to the thermal expansion of the beam introduces P-Δ effects and reduces the capacity of the column. This reduced capacity contributes to the global structural collapse of the left half of the building, since the reduction in the column axial capacity converts the beams of the left bay of the building to cantilever beams (supported on the wall). The columns in the Cardington fire tests exhibited similar outward deflections due to the thermal expansion of the slabs. Modeling this global behavior is critical in designing structures to resist earthquake and fire effects. Being able to model the global behavior allows the design to take advantage of beneficial mechanisms (such as tension or compression membranes or load redistribution) and also to detect and potentially alleviate mechanisms that may cause negative impacts on structural performance (such as outward column displacement).

6 Summary and Discussion

Post-earthquake fires can be a serious hazard to RC structures, sometimes causing more damage than the earthquake itself, and tools must be developed to analyze structures for this scenario. This study has presented a nonlinear truss method for RC structures that can incorporate both cyclic earthquake loading and elevated-temperature behavior due to fire. This method is an enhancement of an existing truss method that has been validated for earthquake loading. Existing constitutive models are enhanced so that the effects of elevated temperature on strength, deformability, and strain are incorporated. The proposed enhanced nonlinear truss method has been validated using existing experimental data on the material-level behavior of concrete and reinforcing steel at elevated temperatures. The ability of the proposed method to capture system-level behavior has also been verified.

The validation analyses showed good agreement for the stress-strain behavior of concrete and steel at elevated temperatures. For concrete behavior at temperatures above 550°C, a modification was made to the transient strain formulation to capture better the stress-strain behavior. The proposed model adequately captures the reduction in strength and initial slope of the steel stress-strain curves, but it does not capture the loss of yield plateau for monotonic loading. In the case of a post-earthquake fire, the steel will likely enter the strain hardening region during the earthquake loading. Once in the strain hardening region, the stress-strain curve is nonlinear, and this will account for the loss of the yield plateau.

The validation analysis comparing the strain behavior of concrete at elevated temperatures shows that the proposed model is capable of capturing strain contributions due to thermal, mechanical, and transient strains. Better agreement could be obtained in future studies by using a formulation for thermal strain that is specific to the type of aggregate used in testing.

Additionally, a new formulation for transient strain at temperatures greater than 550°C may provide better estimates for specimens subjected to such temperatures.

The verification analyses demonstrate the capabilities of the proposed model in predicting system-level structural behavior when subjected to earthquake or fire effects. The model captures global mechanisms that have been observed in prior experimental testing, such as membrane behavior and outward displacement of columns due to thermal expansion. The heat conduction functionality is able to predict the spread of heat throughout a structure, but further development is needed in the future.

One of the advantages of the method described herein is that the enhancements to account for the effect of elevated temperature do not require modifications of the core constitutive law. The described methods for incorporating the transient and thermal strains and for reducing the stress due to temperature effects can be combined with existing cyclic constitutive laws that are developed for earthquake analysis. The transient and thermal strains are significant portions of the total strain at elevated temperatures and cannot be neglected in an analysis.

The material models formulated here for combined mechanical and thermal effects are based on uniaxial stress-strain laws, which are conceptually simpler and computationally more efficient than the multi-axial constitutive laws typically used in refined finite element models. Test data, particularly for cyclic loading and elevated temperature effects, is more readily available for uniaxial loading conditions, making it easier to apply the truss model to different types of materials and conditions. Additionally, the axial-flexure-shear interaction is naturally captured at the material level in the truss method, so calibration of nonlinear springs to capture the effect of shear damage is not required, as is the case with beam models. The computational

efficiency of the proposed truss method allows for extensive parametric analyses that can aid in the development of design guidelines for combined earthquake and fire effects.

7 Recommendations for Future Research

While there has been much research on earthquake and fire effects individually, experimental and analytical research on the combined effects of earthquake and fire on structures is lacking. Very few experimental studies are available to use for calibration of analytical models. Experimental tests evaluating the performance of single structural elements (e.g. beams or columns) under combined earthquake and fire effects will be useful for both calibration of analytical models and investigating appropriate design guidelines. Full-scale studies of structures subjected to earthquake loading followed by fire will also be integral to understanding the system-level behavior.

One of the aspects of the concrete behavior at elevated temperatures that is difficult to capture accurately is the transient strain at temperatures above 550°C. The formulation proposed in prior research and used in the enhanced truss model appears to over predict the transient strain when compared to existing test data. Due to the large scatter in the concrete strains, particularly at higher temperatures, it is difficult to develop a formulation that can adequately capture the behavior. More research into transient strain at temperatures above 550°C is critical for developing a more accurate and comprehensive formulation.

In future work, the proposed truss method could be coupled with Fire Dynamics Simulator (FDS), which is a computational fluid dynamics program developed by the National Institute of Standards and Technology (NIST). FDS is capable of accurately modeling fire spread throughout a structure due to diffusion and advection and would provide a more rigorous heat transfer analysis than what is presently incorporated in the FEAP model. When the two programs

are coupled, the temperature distribution at each time step would be predicted by FDS, and those temperatures would be used in the proposed truss model to perform the mechanical analysis.

In future research, the proposed enhanced nonlinear truss model can be extended to include the effects of thermal spalling due to water vapor pressure at high temperatures. While the current model can account for spalling during earthquakes and spalling due to thermal restraint, it cannot account for spalling due to high water vapor pressure. This aspect could be incorporated into the proposed model using reduction factors, similar to the methods used for the strength reduction factors. When multiplied by the cross-sectional area of the truss member, a spalling reduction factor could take into account the loss of concrete due to spalling caused by high water vapor pressure. The value of the reduction factor should depend on parameters that affect the probability of spalling, such as tensile strength of concrete, rate of temperature rise, and permeability of concrete.

The proposed nonlinear truss method is applicable for uniaxial truss elements, but in the future, the methods for incorporating thermal effects on the stress-strain laws can be extended to multiaxial stress-strain laws. The simplest method for incorporating this is to use a principal stress coordinate system. Specifically, the stress reduction factors and the increments in temperature-induced strains (thermal strain, transient strain) can be calculated for each principal direction. The corresponding principal stress value can be used in the equation for the transient strain. This extension would allow for coupled thermo-mechanical simulations in cases where the triaxial stress states in the material are important. One such case is two-way beam-to-column joints in reinforced concrete frame buildings.

Additional research is needed in the area of design provisions for combined earthquake and fire effects. Currently, no design guidelines are available, and simplified models are not available for use in performance-based design. The post-earthquake fire (PEF) factor proposed by Behnam and Ronagh (2014b) is one example that could be investigated further to determine its feasibility for new design guidelines. Continued research on the differences between fire- or earthquake-only damage and the damage due to the combined effects should be pursued. This would allow for a more thorough understanding of the structural behavior and of the requirements necessary for design guidelines.

References

"ABAQUS." (2006). Dassault Systèmes Simulia Corporation, Providence, RI.

ACI, and TMS. (2014). *Code requirements for determining fire resistance of concrete and masonry construction assemblies*. American Concrete Institute.

Anderberg, Y., and Thelandersson, S. (1976). "Stress and deformation characteristics of concrete at high temperatures: 2. Experimental investigation and material behaviour model." Lund, Sweden.

ASCE Committee on Fire Protection. (1992). "ASCE Manual No. 78: Structural Fire Protection."

ASTM. (2014). "E119-14 Standard test methods for fire tests of building construction and materials."

Bailey, C. (2002). "Holistic behaviour of concrete buildings in fire." *Proceedings of the ICE - Structures and Buildings*, 152(3), 199–212.

Bamonte, P., and Lo Monte, F. (2015). "Reinforced concrete columns exposed to standard fire : Comparison among different constitutive models for concrete at high temperature." *Fire Safety Journal*, 71, 310–323.

Bažant, Z. P., and Kaplan, M. F. (1996). *Concrete at High Temperatures: Material Properties and Mathematical Models*. Longman, Harlow.

Behnam, B., and Ronagh, H. (2014a). "A study on the effect of sequential post-earthquake fire on the performance of reinforced concrete structures." *International Journal of Structural Integrity*, 5(2), 141–166.

Behnam, B., and Ronagh, H. (2014b). "An Engineering Solution to Improve Post-Earthquake Fire Resistance in Important Reinforced Concrete Structures." *Advances in Structural Engineering*, 17(7), 993–1009.

Bhargava, P., Kamath, P., Usmani, A., May, I., B Singh, B., Gillie, M., Sharma, U. K., Kumar, V., Pankaj, P., Torero, J., Y Singh, Y., and Zhang, J. (2012). "Full-scale testing of a damaged reinforced concrete frame in fire." *Proceedings of the ICE - Structures and Buildings*, 165, 335–346.

Biondini, F., and Nero, A. (2011). "Cellular Finite Beam Element for Nonlinear Analysis of Concrete Structures under Fire." *Journal of Structural Engineering*, 137(5), 543–558.

Chana, P., and Price, B. (2003). "The Cardington Fire Tests." *Concrete*, 37(1), 28–33.

Dodd, L. L., and Restrepo-Posada, J. I. (1995). "Model for Predicting Cyclic Behavior of Reinforcing Steel." *Journal of Structural Engineering*, 121(3), 433–445.

Dwaikat, M. B., and Kodur, V. K. R. (2008). *SP-255-6 Comparisons of Fire Resistance of RC Beams from Different Codes of Practice*.

European Committee for Standardization. (2002). *Eurocode 1: Actions on Structures - Part 1-2: General actions - Actions on structures exposed to fire*.

European Committee for Standardization. (2004). *Eurocode 2: Design of concrete structures - Part 1-2: General rules - Structural fire design*.

FEMA. (2012). *FEMA P-751: 2009 NEHRP Recommended Seismic Provisions: Design Examples*.

Harmathy, T. Z., and Stanzak, W. W. (1970). *Elevated-Temperature Tensile and Creep Properties of Some Structural and Prestressing Steels*. *Fire Test Performance, ASTM STP 464*.

Hughes, T. J. R. (2000). *The Finite Element Method: Linear Static and Dynamic Finite Element Analysis*. Dover Publications, Mineola, NY.

International Code Council. (2015). "International Building Code."

Kim, S. (2014). "Cyclic Uniaxial Constitutive Model for Steel Reinforcement." Virginia Tech.

Kirby, B. R., and Preston, R. R. (1988). "High temperature properties of hot-rolled, structural steels for use in fire engineering design studies." *Fire Safety Journal*, 13(1), 27–37.

Knaack, A. M., Kurama, Y. C., and Kirkner, D. J. (2009). *Stress-Strain Properties of Concrete at Elevated Temperatures, Report #NDSE-09-01*. *Structural Engineering Research Report*.

Knaack, A. M., Kurama, Y. C., and Kirkner, D. J. (2011). "Compressive stress-strain relationships for North American concrete under elevated temperatures." *ACI Materials Journal*, 108(3), 270–280.

Kodur, V., Dwaikat, M., and Raut, N. (2009). "Macroscopic FE model for tracing the fire response of reinforced concrete structures." *Engineering Structures*, 31, 2368–2379.

Kodur, V. K. R. (2008). *SP-255-5 Fire Resistance of Reinforced Concrete Columns – State-of-the-Art and Research Needs*.

Kodur, V. K. R., Dwaikat, M. M. S., and Dwaikat, M. B. (2008). "High-temperature properties of concrete for fire resistance modeling of structures." *ACI Materials Journal*, 105(5), 517–527.

Koutromanos, I. (2011). "Numerical Analysis of Masonry-Infilled Reinforced Concrete Frames Subjected to Seismic Loads and Experimental Evaluation of Retrofit Techniques." University of California, San Diego.

Li, L. Y., and Purkiss, J. (2005). "Stress-strain constitutive equations of concrete material at elevated temperatures." *Fire Safety Journal*, 40, 669–686.

Massone Sanchez, L. M. (2006). "RC Wall Shear-Flexure Interaction: Analytical and Experimental Responses." University of California, Los Angeles.

Moharrami, M., Koutromanos, I., Panagiotou, M., and Girgin, S. C. (2014). "Analysis of shear-dominated RC columns using the nonlinear truss analogy." *Earthquake Engineering & Structural Dynamics*.

Mousavi, S., Bagchi, A., and Kodur, V. K. R. (2008). "Review of post-earthquake fire hazard to building structures." *Canadian Journal of Civil Engineering*, 35(November), 689–698.

Panagiotou, M., Restrepo, J. I., Schoettler, M., and Kim, G. (2012). "Nonlinear Cyclic Truss Model for reinforced concrete walls." *ACI Structural Journal*, 109(2), 205–214.

Parkinson, D., Kodur, V., and Sullivan, P. (Eds.). (2008). *ASCE Manual No. 114: Performance-Based Design of Structural Steel for Fire Conditions*. American Society of Civil Engineers.

Phan, L. T., McAllister, T. P., Gross, J. L., and Hurley, M. J. (Eds.). (2010). "Best practice guidelines for structural fire resistance design of concrete and steel buildings."

Purkiss, J. A., and Li, L.-Y. (2013). *Fire Safety Engineering Design of Structures*. CRC Press.

Raut, N., and Kodur, V. (2011). *SP-279-10 Computer Model for Predicting the Fire Response of Reinforced Concrete Columns*.

Rini, D., Gerard, R., Almufti, I., and Nielson, G. (2011). "Structural Fire Engineering for Modern Building Design- Case Study." *Proceedings, AEI 2011: Building Integration Solutions*, 351–360.

Rini, D., and Lamont, S. (2008). "Performance based structural fire engineering for modern building design." *Proc., 2008 Structures Congress*.

Sadaoui, A., and Khennane, A. (2009). "Effect of transient creep on the behaviour of reinforced concrete columns in fire." *Engineering Structures*, 31, 2203–2208.

Sittipunt, C., Wood, S. L., Lukkunaprasit, P., and Pattararattanakul, P. (2001). "Cyclic Behavior of Reinforced Concrete Structural Walls with Diagonal Web Reinforcement." *ACI Structural Journal*, 98(4), 554–562.

Standards Australia Committee BD-002. (2009). *AS 3600: Concrete Structures*.

Steel Construction Manual. (2011). American Institute of Steel Construction.

Taylor, R. L. (2013). "Finite Element Analysis Program." University of California, Berkeley.

Ulm, F., Acker, P., and Levy, M. (1999). "The 'Chunnel' Fire II: Analysis of Concrete Damaga." *Journal of Engineering Mechanics*, 125(3), 283–289.

Vecchio, F. J., and Collins, M. P. (1986). "The Modified Compression Field Theory for Reinforced Concrete Elements Subjected to Shear." *ACI Journal Proceedings*, 83(2).

Wang, Y., Burgess, I., Wald, F., and Gillie, M. (2013a). *Performance-Based Fire Engineering of Structures*. CRC Press, Boca Raton, FL.

Wang, Y., Dong, Y. L., and Zhou, G. C. (2013b). "Nonlinear numerical modeling of two-way reinforced concrete slabs subjected to fire." *Computers and Structures*, 119, 23–36.

Youssef, M. A., El-Fitiany, S. F., and Elfeki, M. A. (2008). *SP-255-3 Flexural Behavior of Protected Concrete Slabs after Fire Exposure*.

Youssef, M. a., and Moftah, M. (2007). "General stress-strain relationship for concrete at elevated temperatures." *Engineering Structures*, 29, 2618–2634.

Zaidi, K. a., Sharma, U. K., and Bhandari, N. M. (2012). "Effect of temperature on uni-axial compressive behavior of confined concrete." *Fire Safety Journal*, 48, 58–68.